An International Journal of Optimization and Control: Theories & Applications
ISSN: 2146-0957 eISSN: 2146-5703
Vol.16, No.6, pp.2399-2423 (2026)
https://doi.org/10.36922/IJOCTA026330212

RESEARCH ARTICLE

Dynamical features and dispersive soliton solutions of a fractional extended Schrödinger model incorporating cubic-quadratic nonlinear terms

Shafqat Ur Rehman[1,2], Sekson Sirisubtawee[1,3*], Khomsan Neamprem[1,3], and Chaiyod Kamthorncharoen[1,3]

[1]Department of Mathematics, Faculty of Applied Science, King Mongkut's University of Technology North Bangkok, Bangkok, Thailand
[2]Department of Mathematics, Grand Asian University, Sialkot, Pakistan
[3]Centre of Excellence in Mathematics, MHESI, Bangkok, Thailand
shafqatrehman2005@yahoo.com, sekson.s@sci.kmutnb.ac.th, khomsan.n@sci.kmutnb.ac.th, chaiyod.k@sci.kmutnb.ac.th

ARTICLE INFO

Article history:
Received: August 13, 2026
Revised: September 11, 2026
Accepted: September 18, 2026
Published Online: October 12, 2026

Keywords:
Soliton solutions
M-truncated extended NLS equation
ERSC–SHC method
GERFM
Modulation instability
Sensitivity analysis
Bifurcation and chaos

AMS Classification 2020:
35R11; 35C07; 35C08
34C23; 35Q55

ABSTRACT

This study is devoted to investigating soliton solutions and qualitative analysis of the M-fractional extended nonlinear Schrödinger (NLS) equation with cubic-quadratic nonlinear terms. This research is motivated by the significance of the extended NLS model in optics, quantum mechanics, plasma physics, electromagnetic wave propagation, and the approximate description of dense quasi-one-dimensional Bose–Einstein condensates (BECs) involving repulsive contact interactions and long-range dipole-dipole attraction. The research gap concerns the limited understanding of the combined solitonic, modulational, and dynamical characteristics of this fractional cubic-quadratic model. The novelty lies in integrating the extended rational sine-cosine/sinh-cosh (ERSC–SHC) and generalized exponential rational function (GERFM) methods with modulation instability (MI), sensitivity analysis, bifurcation analysis, and chaos analysis. The contributions include bright, dark, singular, periodic, and exponential soliton structures in single and combined forms, MI regions obtained through linear stability theory, and qualitative analysis supported by graphical representations and phase portraits. A comparative analysis demonstrates distinct dynamical features, providing a foundation for investigations of nonlinear wave propagation and BEC dynamics.

CC BY

1. Introduction

The dynamics of nonlinear phenomena across applied sciences have attracted significant attention due to their importance in explaining and studying complicated natural processes, underlining the significance of developing nonlinear equations to enrich our understanding in fields such as physics, applied mathematics, and engineering. Across engineering, modeling and investigating such phenomena often relies on nonlinear partial differential equations (NLPDEs). The rigorous mathematical analysis of nonlinear processes is widely regarded as an intricate and inspiring undertaking, often requiring sophisticated numerical and computational methods or specialized analytical techniques. In order to achieve more realistic and accurate models, it is essential to take into account nonlinear phenomena, since they play a very important role in dealing with complex phenomena. Thus, models involving strong mathematical structures, particularly those including differential equations, are generally employed to

*Corresponding Author

mathematically describe many nonlinear phenomena. In this sense, the importance of NLPDEs cannot be overlooked, since they offer a powerful and flexible method for dealing with a wide range of problems.[1–4]

The search for exact and analytical solutions for NLPDEs is vital, as it offers insights into the mechanisms of nonlinear phenomena. Recently, many researchers have studied NLPDEs in order to find classes of soliton solutions. For this reason, researchers have achieved significant results in developing solutions for NLPDEs using various analytical and numerical techniques. Among various methods, many powerful and effective analytical methods exist, including the $(\frac{G'}{G^2})$-expansion function method,[5] the extended rational sinh-Gordon equation technique,[6,7] the Hirota bilinear approach,[8] the modified extended direct algebraic scheme,[9] the improved F-expansion function method,[10] the improved Adomian decomposition method,[11] the $(\frac{G'}{G}, \frac{1}{G})$-expansion function method,[12] the extended trial equation mechanism,[13] the modified Kudryashov method,[14] the generalized Riccati equation method,[15] and various other techniques.[16–19] These prolific and efficient approaches, devoted to constructing soliton solutions for NLPDEs, continue to evolve.

On the other hand, solitons are of prime importance in the optical fiber communication systems because of their extraordinary robustness, polarization and dispersion insensitivity, and particle-like properties when exposed to perturbations. These localized one-pulse structures are the backbone of contemporary fiber optic communication systems, which are capable of transmitting data over long distances with only a slight change in the pulse shape. Solitons, which arise from the delicate interplay of nonlinearity and dispersion, maintain their form and velocity as they propagate, rendering them significant for the study of nonlinear waves in optics, fluids, and plasmas. However, in the current scenario, the study of solitons has not only become a hot topic among physicists and mathematicians due to the unique feature of solitons, which is the preservation of their shapes, but it has also become a promising area for exploration due to its potential impact on high-speed optical communication systems and optical switching systems. Different analytical and numerical methods have been considered by scholars to address the issues related to NLPDEs for such systems.[20–23] Among such systems, the NLS equation is regarded as prominent equation, widely used for the description of various systems, as well as for the simulation of the complex interactions between the impacts of dispersion and nonlinearity, for the interpretation of the evolution of nonlinear solitons over transcontinental and transoceanic distances. In addition to nonlinear optics, the NLS equation is used for the description of an exceptional structure for the study of various physical phenomena, such as the propagation of waves in dispersive or inhomogeneous media, biomolecular dynamics, and surface waves in deep ocean waters. The flexibility of this equation enables both analytical and computational assessment of complex behaviors, including solitons, breathers, and rogue waves. In practical frameworks, the NLS equation is instrumental in optimizing high-capacity optical communication systems and advancing signal-processing technologies. Many different forms of the NLS equation that can be found in the literature, for example, the higher-order NLS equation, the Fokas-Lenells (FL) equation, the Ginzburg-Landau (GL) equation, etc. For example, the one-dimensional derivative NLS equation describes the propagation of nonlinear waves in nonlinear optics, plasma, BEC, etc. Quadratic–cubic nonlinearity develops in systems with strong nonlinear interactions and encourages rich soliton dynamics.[24–26]

The extended NLS equation model with cubic-quadratic nonlinearity is given in[27] as

$$\begin{aligned} iD_{M,t}^{\alpha,\beta}\Psi + aD_{M,x}^{2\alpha,\beta}\Psi - b_1|\Psi|\Psi + b_2|\Psi|^2\Psi = 0, \\ \alpha \in (0,1], \;\; \beta > 0. \end{aligned} \tag{1}$$

Here, $\Psi(x,t)$ represents a complex-valued function that is a dependent variable, whereas x and t are independent variables that signify spatial and temporal variables, respectively. $D_{M,t}^{\alpha,\beta}(\cdot)$ and $D_{M,x}^{2\alpha,\beta}(\cdot)$ are the M-fractional derivatives of order α with respect to t and of order 2α with respect to x, respectively. The parameter a signifies the group velocity dispersion, while b_1 and b_2 correspond to the quadratic and cubic nonlinear parts, respectively. The leading term describes the linear evolution of the soliton pulse. This model has been the subject of extensive theoretical and numerical study. Recently, in,[27] the investigators used the method of undetermined coefficients to obtain exact solutions and conservation laws of the governing model. The authors of[28] obtained chirped similar waves by employing the similarity transformation method. J. Fujioka *et al.*[29] discussed the chaotic solitons of the model. Furthermore, various analytical techniques have been implemented to examine the equation,such as He's semi-inverse variational principle in,[30] the Jacobi elliptic function ansatz method in,[31] and the sine-Gordon expansion approach in.[32] Finally, the modified Khater method and the generalized

$\exp(-\phi(\xi))$-expansion method were applied in[33] to find some soliton solutions.

In recent years, bifurcation, sensitivity, and control analyses have been identified as crucial aspects in the study of complex nonlinear dynamical systems. For example, research on bifurcation and control analysis in predator-prey systems with two delays[34] has illustrated the impact of delay parameters on the stability and qualitative features of nonlinear systems. Likewise, analysis of Hopf bifurcation and control in delay systems[35] has provided important insights into oscillations and their control in these systems. Such advancements have further underscored the need to analyze parameter-dependent stability and dynamical responses of nonlinear systems. Stimulated by such research efforts, this research analyzes sensitivity, bifurcation, and chaos in the chosen M-fractional extended nonlinear Schrödinger equation.

A survey of previous findings shows that the extended NLS equation with cubic-quadratic nonlinearity has not been analyzed using the extended rational sine-cosine/sinh-cosh (ERSC–SHC) method[36] or the generalized exponential rational function method (GERFM).[37] Furthermore, none of the previous investigators have analyzed sensitivity, bifurcation analysis, and chaos. In,[32] the authors derived the modulation instability of the stated model without using any fractional derivatives. However, in this present study, we derive the modulation instability by using the M-truncated fractional derivative. This observation addresses a significant gap in the earlier literature. This study intends to address this gap by utilizing these approaches. The GERFM is a powerful analytical technique that facilitates the derivation of exact soliton solutions such as bright, dark, and singular solitons, kink-type, and periodic waves for complex NLPDEs, including those with fractional derivatives. Similarly, new extended forms of rational trigonometry, such as the rational sine-cosine method or the sinh-cosh method, improve existing frameworks for systematically developing a wider range of solutions for describing of various physical phenomena in fields such as fiber optics, fluid dynamics, and plasma physics.

The remaining parts of the paper are organized as follows. Section 2 discusses the M-truncated fractional derivative and its properties. In Section 3, the techniques are implemented. The graphical interpretation of selected soliton solutions is presented in Section 4. Section 5 sheds light on the modulation instability (MI) analysis. Sections 6–8 demonstrate qualitative analyses of the studied model. In Section 9, the comparison and novelty of the study are presented. Finally, we conclude our findings in Section 10.

2. *M*-truncated derivative

Fractional calculus has been recognized as a powerful tool for accurate modeling of a broad range of physical phenomena. The fractional-order model presents greater adaptability and flexibility in comparison to traditional integer-order models, thus providing greater applicability in dealing with complex systems. This article aims to cover the basic concepts of fractional derivatives, which are considered crucial in understanding and dealing with the dynamics of physical systems.[38,39] The M-truncated derivative presents a significant advantage in dealing with the dynamics of complex systems, thus differentiating it from traditional fractional calculus. In addition, it facilitates the isolation and analysis of particular intervals, providing innate insights into fundamental physical phenomena. The M-truncated derivative is preferred due to its distinct method of fractional differentiation. It selectively reduces the integral part for prescribed fractional orders, hence lowering computational complexity while maintaining numerical stability and efficiency. This renders it a feasible technique for the derivation of soliton solutions for the nonlinear model under investigation. Some properties of the M-truncated derivative are provided below.

Definition: Let $h(x) : [0, \infty) \to \Re$. The M-fractional derivative of $h(x)$ of order α[40,41] is

$$D_{M,x}^{\alpha,\beta} h(x) = \lim_{\epsilon \to 0} \frac{h(xE_\beta(\epsilon x^{-\alpha})) - h(x)}{\epsilon}, \qquad \alpha \in (0,1],\ \beta > 0,$$

where $E_\beta(.)$ signifies a truncated Mittag-Leffler function[39]

$$E_\beta(z) = \sum_{k=0}^{l} \frac{z^k}{\Gamma(\beta k + 1)}, \qquad \text{where} \quad z \in C.$$

Characteristics: Let $a, b \in \Re$ and p, q be α-differentiable at a point $x > 0$, then

$(i)\ D_{M,x}^{\alpha,\beta}(ap(x) + bq(x)) = aD_{M,x}^{\alpha,\beta} p(x) + bD_{M,x}^{\alpha,\beta} q(x),$

$(ii)\ D_{M,x}^{\alpha,\beta}(p(x).q(x)) = p(x)D_{M,x}^{\alpha,\beta} q(x) + q(x)D_{M,x}^{\alpha,\beta} p(x),$

$$(iii)\ D_{M,x}^{\alpha,\beta} \frac{p(x)}{q(x)} = \frac{q(x)D_{M,x}^{\alpha,\beta} p(x) - p(x)D_{M,x}^{\alpha,\beta} q(x)}{(q(x))^2},$$

$(iv)\ D_{M,x}^{\alpha,\beta}(c) = 0,$ where c is a constant,

$$(v)\ D_{M,x}^{\alpha,\beta}(p(x)) = \frac{x^{1-\alpha}}{\Gamma(\beta+1)} \frac{dp(x)}{dx}.$$

3. Mathematical analysis

In this part, we aim to retrieve several soliton solutions for the present model. To convert **Equation (1)** into an ordinary differential equation, we utilize the following wave transformations:

$$\Psi(x,t) = \Upsilon(\zeta)e^{i\Theta},$$
$$\zeta = \frac{\Gamma(\beta+1)}{\alpha}(x^\alpha - \nu t^\alpha), \quad \text{and}$$
$$\Theta = \frac{\Gamma(\beta+1)}{\alpha}(-\kappa x^\alpha + \omega t^\alpha) + \theta_0. \tag{2}$$

Substituting the transformation (2) into **Equation (1)**, **Equation (1)** can be decomposed into the real part

$$a\Upsilon'' + b_2\Upsilon^3 - b_1\Upsilon^2 - (a\kappa^2+\omega)\Upsilon = 0, \tag{3}$$

and the imaginary part

$$\nu = -2a\kappa. \tag{4}$$

3.1. Implementation of extended rational sine-cosine method

Assume the trial solution for **Equation (3)** according to the extended rational sine-cosine method is

$$\Upsilon(\zeta) = \frac{\beta_0 \sin(\zeta\phi)}{\beta_1 \cos(\zeta\phi) + \beta_2}, \qquad \cos(\zeta\phi) \neq -\frac{\beta_2}{\beta_1}, \tag{5}$$

where β_0, β_1 and β_2 are constants which will be determined later. Substituting **Equation (5)** and its derivative into **Equation (3)** yields an expression in $\cos(\zeta\phi)$. Setting each attained coefficient of $\cos(\zeta\phi)$ to zero leads to the following sets of solutions:

Set-1

$$\phi = \frac{\sqrt{2}\sqrt{a\kappa^2+\omega}}{\sqrt{a}},\ \beta_0 = \frac{i\beta_1\sqrt{a\kappa^2+\omega}}{\sqrt{b_2}},\ \beta_2 = -\beta_1,$$
$$b_1 = 0, \quad \text{where } a, b_2 \neq 0.$$

Set-2

$$\phi = \frac{\sqrt{a\kappa^2+\omega}}{\sqrt{2}\sqrt{a}},\ \beta_0 = \frac{i\beta_1\sqrt{a\kappa^2+\omega}}{\sqrt{b_2}},\ \beta_2 = 0, b_1 = 0,$$

where $a,\ b_2 \neq 0$.

From the values of coefficients in Set-1 above, we formulate the complex periodic solution:

$$\Psi_1(x,t) = \left(-\frac{i\sqrt{a\kappa^2+\omega}\cot\left(\frac{\sqrt{a\kappa^2+\omega}(\zeta)}{\sqrt{2}\sqrt{a}}\right)}{\sqrt{b_2}}\right) \times e^{i\left(\theta_0 + \frac{\Gamma(\beta+1)(\omega t^\alpha - \kappa x^\alpha)}{\alpha}\right)}. \tag{6}$$

From the values of coefficients in Set-2 above, we construct the complex trigonometric solution:

$$\Psi_2(x,t) = \left(\frac{i\sqrt{a\kappa^2+\omega}\tan\left(\frac{\sqrt{a\kappa^2+\omega}(\zeta)}{\sqrt{2}\sqrt{a}}\right)}{\sqrt{b_2}}\right) \times e^{i\left(\theta_0 + \frac{\Gamma(\beta+1)(\omega t^\alpha - \kappa x^\alpha)}{\alpha}\right)}. \tag{7}$$

OR

Assume the trial solution for **Equation (3)** in the following form

$$\Upsilon(\zeta) = \frac{\beta_0 \cos(\zeta\phi)}{\beta_1 \sin(\zeta\phi) + \beta_2}, \qquad \sin(\zeta\phi) \neq -\frac{\beta_2}{\beta_1}, \tag{8}$$

where β_0, β_1 and β_2 are constants which will be determined later. On substituting **Equation (8)** and its derivative into **Equation (3)**, an expression involving the exponent of $\sin(\zeta\phi)$ is obtained. By setting each exponent of $\sin(\zeta\phi)$ to zero, the following sets of solutions are found:

Set-3

$$\phi = \frac{\sqrt{2}\sqrt{a\kappa^2+\omega}}{\sqrt{a}},\ \beta_0 = \frac{i\beta_1\sqrt{a\kappa^2+\omega}}{\sqrt{b_2}},\ \beta_2 = -\beta_1,$$
$$b_1 = 0, \quad \text{where } a, b_2 \neq 0.$$

Then we obtain the solution from Set-3 as

$$\Psi_3(x,t) = \left(\frac{i\sqrt{a\kappa^2+\omega}\cos\left(\frac{\sqrt{2}\sqrt{a\kappa^2+\omega}(\zeta)}{\sqrt{a}}\right)}{\sqrt{b_2}\left(\sin\left(\frac{\sqrt{2}\sqrt{a\kappa^2+\omega}(\zeta)}{\sqrt{a}}\right)-1\right)}\right) \times e^{i\left(\theta_0 + \frac{\Gamma(\beta+1)(\omega t^\alpha - \kappa x^\alpha)}{\alpha}\right)}. \tag{9}$$

3.2. Implementation of extended rational sinh-cosh method

Assume the trial solution for **Equation (3)** according to the rational sinh-cosh method is

$$\Upsilon(\zeta) = \frac{\beta_0 \sinh(\zeta\phi)}{\beta_1 \cosh(\zeta\phi) + \beta_2}, \quad \cosh(\zeta\phi) \neq -\frac{\beta_2}{\beta_1}, \tag{10}$$

where β_0, β_1 and β_2 are constants to be determined later. Substituting **Equation (10)** and its derivative into **Equation (3)** yields an expression involving the power of $\cosh(\zeta\phi)$. By setting each power of $\cosh(\zeta\phi)$ to 0, the following sets of solutions are found:

Set-4

$$\phi = \frac{\sqrt{2}\sqrt{-a\kappa^2-\omega}}{\sqrt{a}},\ \beta_0 = \frac{\beta_1\sqrt{a\kappa^2+\omega}}{\sqrt{b_2}},\ \beta_2 = -\beta_1,$$
$$b_1 = 0, \quad \text{where } a, b_2 \neq 0.$$

Set-5

$$\phi = \frac{\sqrt{2}\sqrt{-a\kappa^2-\omega}}{\sqrt{a}},\ \beta_1 = \frac{\sqrt{b_2}\beta_0}{\sqrt{a\kappa^2+\omega}},$$
$$\beta_2 = \frac{\sqrt{b_2}\beta_0}{\sqrt{a\kappa^2+\omega}},\ b_1 = 0,$$

where $a,\ a\kappa^2+\omega \neq 0$.

From the values of the coefficients in Set-4 and Set-5 above, we extract singular and dark soliton solutions, respectively.

$$\Psi_4(x,t) = \left(\frac{\sqrt{a\kappa^2+\omega}\coth\left(\frac{\sqrt{-a\kappa^2-\omega}(\zeta)}{\sqrt{2}\sqrt{a}}\right)}{\sqrt{b_2}}\right) \times e^{i\left(\theta_0 + \frac{\Gamma(\beta+1)(\omega t^\alpha - \kappa x^\alpha)}{\alpha}\right)}. \tag{11}$$

$$\Psi_5(x,t) = \left(\frac{\sqrt{a\kappa^2+\omega}\tanh\left(\frac{\sqrt{-a\kappa^2-\omega}(\zeta)}{\sqrt{2}\sqrt{a}}\right)}{\sqrt{b_2}}\right) \times e^{i\left(\theta_0+\frac{\Gamma(\beta+1)(\omega t^\alpha-\kappa x^\alpha)}{\alpha}\right)}. \quad (12)$$

OR

Assume the trial solution for **Equation (3)** in the following form

$$\Upsilon(\zeta) = \frac{\beta_0\cosh(\zeta\phi)}{\beta_1\sinh(\zeta\phi)+\beta_2}, \quad \sinh(\zeta\phi) \neq -\frac{\beta_2}{\beta_1}, \quad (13)$$

where β_0, β_1 and β_2 are constants to be determined later. Substituting **Equation (13)** and its derivative into **Equation (3)** yields an expression in $\sinh(\zeta\phi)$. By setting each power of $\sinh(\zeta\phi)$ to zero, we obtain the following sets of solutions:

Set-6

$$\phi = \frac{\sqrt{2}\sqrt{-a\kappa^2-\omega}}{\sqrt{a}},\ \beta_0 = \frac{i\beta_2\sqrt{a\kappa^2+\omega}}{\sqrt{b_2}},$$
$$\beta_1 = -i\beta_2,\ b_1 = 0, \text{ where } a, b_2 \neq 0.$$

Set-7

$$\phi = \frac{\sqrt{2}\sqrt{-a\kappa^2-\omega}}{\sqrt{a}},\ \beta_1 = \frac{\sqrt{b_2}\beta_0}{\sqrt{a\kappa^2+\omega}},$$
$$\beta_2 = \frac{\sqrt{b_2}\beta_0}{\sqrt{-a\kappa^2-\omega}},\ b_1 = 0, \text{ where } a,\ a\kappa^2+\omega \neq 0.$$

From the values of the coefficients in Set-6 and Set-7 above, we attain mixed hyperbolic solutions, respectively.

$$\Psi_6(x,t) = \left(-\frac{\sqrt{a\kappa^2+\omega}\cosh\left(\frac{\sqrt{2}\sqrt{-a\kappa^2-\omega}(\zeta)}{\sqrt{a}}\right)}{\sqrt{b_2}\left(\sinh\left(\frac{\sqrt{2}\sqrt{-a\kappa^2-\omega}(\zeta)}{\sqrt{a}}\right)+i\right)}\right) \times e^{i\left(\theta_0+\frac{\Gamma(\beta+1)(\omega t^\alpha-\kappa x^\alpha)}{\alpha}\right)}. \quad (14)$$

$$\Psi_7(x,t) = \left(\frac{\sqrt{-(a\kappa^2+\omega)^2}\cosh\left(\frac{\sqrt{2}\sqrt{-a\kappa^2-\omega}(\zeta)}{\sqrt{a}}\right)}{\sqrt{b_2}\left(\sqrt{a\kappa^2+\omega}+\sqrt{-a\kappa^2-\omega}\sinh\left(\frac{\sqrt{2}\sqrt{-a\kappa^2-\omega}(\zeta)}{\sqrt{a}}\right)\right)}\right) \times e^{i\left(\theta_0+\frac{\Gamma(\beta+1)(\omega t^\alpha-\kappa x^\alpha)}{\alpha}\right)}. \quad (15)$$

Remark: **Limitation of the ERSC-SHC solution families**: It is important to note that all eight parameter sets generated by the ERSC-SHC method satisfy $b_1 = 0$. Hence, these solution families correspond to the cubic-NLS limiting case of the proposed quadratic-cubic fractional model rather than to the general case ($b_1 \neq 0$). In this limit, **Equation (1)** reduces to $(iD^{\alpha,\beta}_{M,t}\Psi + aD^{2\alpha,\beta}_{M,x}\Psi + b_2|\Psi|^2\Psi = 0)$. Although the quadratic nonlinear term does not exist for the particular sets mentioned above, the solutions obtained are still valid since they constitute fractional cubic-NLS wave solutions, establish a practical limiting case for the proposed model, and enable comparison with the standard theory of cubic nonlinear Schrödinger systems. In this regard, the constraint ($b_1 = 0$) must be seen as a limitation of the current ERSC-SHC approach, rather than a constraint on the underlying equation itself. A thorough description of the quadratic-cubic nonlinear regime can only be achieved by using solution branches with $b_1 \neq 0$.

3.3. GERFM

Assuming the trial solution of **Equation (3)** can be written according to GERFM as follows

$$\Upsilon(\zeta) = \mu_0 + \sum_{j=1}^{N}\mu_j\Lambda(\zeta)^j + \sum_{j=1}^{N}\rho_j\Lambda(\zeta)^{-j}, \quad (16)$$

where

$$\Lambda(\zeta) = \frac{\vartheta_1 e^{\tau_1\zeta} + \vartheta_2 e^{\tau_2\zeta}}{\vartheta_3 e^{\tau_3\zeta} + \vartheta_4 e^{\tau_4\zeta}}. \quad (17)$$

The unknown parameters μ_0, μ_j, ρ_j $(1 \leq j \leq N)$ and constants ϑ_i, τ_i $(1 \leq i \leq 4)$ will be determined, and N will be computed by applying the homogeneous balance formula.

By applying the homogeneous balance formula to Υ'' and Υ^3 in **Equation (3)**, we obtain $N = 1$. Thus, **Equation (16)** becomes

$$\Upsilon(\zeta) = \mu_0 + \mu_1\Lambda(\zeta) + \rho_1\Lambda(\zeta)^{-1}. \quad (18)$$

Family-1: Setting $\vartheta_1 = \vartheta_2 = -1, \vartheta_3 = 1, \vartheta_4 = -1$ and $\tau_1 = 1, \tau_2 = -1, \tau_3 = 1, \tau_4 = -1$, **Equation (17)** becomes

$$\Lambda(\zeta) = -\coth(\zeta). \quad (19)$$

Substituting **Equations (18)** and **(19)** into **Equation (3)**, we obtain a system of algebraic equations. Simplifying it, we obtain the following results:

Result-1:

$$\mu_0 = \frac{6\omega}{b_1\left(\kappa^2-4\right)},\ \mu_1 = 0,\ \rho_1 = \frac{6\omega}{b_1\left(\kappa^2-4\right)},$$
$$b_2 = \frac{b_1^2\left(\kappa^2-4\right)}{18\omega},\ a = -\frac{\omega}{\kappa^2-4},$$

where $b_1\left(\kappa^2-4\right),\ \omega \neq 0$.

Using the coefficients from Result-1, we obtain the corresponding dark soliton.

$$\Psi_8(x,t) = \left(-\frac{6\omega(\tanh(\zeta)-1)}{b_1\left(\kappa^2-4\right)}\right) \times e^{i\left(\theta_0+\frac{\Gamma(\beta+1)(\omega t^\alpha-\kappa x^\alpha)}{\alpha}\right)}. \quad (20)$$

Result-2:

$$\mu_0 = \frac{6\omega}{b_1\left(\kappa^2-4\right)},\ \mu_1 = \frac{6\omega}{b_1\left(\kappa^2-4\right)},\ \rho_1 = 0,$$
$$b_2 = \frac{b_1^2\left(\kappa^2-4\right)}{18\omega},\ a = -\frac{\omega}{\kappa^2-4},$$

where $b_1\left(\kappa^2-4\right),\ \omega \neq 0$.
Using the coefficients from Result-2, we obtain the corresponding singular soliton.

$$\Psi_9(x,t) = \left(-\frac{6\omega(\coth(\zeta)-1)}{b_1\left(\kappa^2-4\right)}\right) \times e^{i\left(\theta_0+\frac{\Gamma(\beta+1)\left(\omega t^\alpha-\kappa x^\alpha\right)}{\alpha}\right)}. \quad (21)$$

Result-3:

$$\mu_0 = -\frac{12\omega}{b_1\left(\kappa^2+8\right)},\ \mu_1 = \frac{i6\sqrt{2}\omega}{b_1\left(\kappa^2+8\right)},$$
$$\rho_1 = -\frac{i6\sqrt{2}\omega}{b_1\left(\kappa^2+8\right)},\ b_2 = -\frac{b_1^2\left(\kappa^2+8\right)}{36\omega},\ a = -\frac{\omega}{\kappa^2+8},$$

where $b_1\left(\kappa^2+8\right),\ \omega \neq 0$.

The coefficients determined in Result-3 yield the following combined soliton solution.

$$\Psi_{10}(x,t) = \left(\frac{6\omega\left(-2-i\sqrt{2}\mathrm{csch}(\zeta)\mathrm{sech}(\zeta)\right)}{b_1\left(\kappa^2+8\right)}\right) \times e^{i\left(\theta_0+\frac{\Gamma(\beta+1)\left(\omega t^\alpha-\kappa x^\alpha\right)}{\alpha}\right)}. \quad (22)$$

Family-2: Setting $\vartheta_1 = i, \vartheta_2 = -i,\ \vartheta_3 = \vartheta_4 = 1$ and $\tau_1 = i,\ \tau_2 = -i,\ \tau_3 = i,\ \tau_4 = -i$, **Equation (17)** becomes

$$\Lambda(\zeta) = -\tan(\zeta). \quad (23)$$

Substituting **Equations (23)** and **(18)** into **Equation (3)** yields a system of algebraic equations, which we solve using Mathematica to obtain the following result.

Result-1:

$$\mu_0 = \frac{2\sqrt{\omega}}{\sqrt{b_2\left(\kappa^2-8\right)}},\ \mu_1 = \frac{\sqrt{2}\sqrt{\omega}}{\sqrt{b_2\left(\kappa^2-8\right)}},$$
$$\rho_1 = \frac{\sqrt{2}\sqrt{\omega}}{\sqrt{b_2\left(\kappa^2-8\right)}},\ b_1 = \frac{6b_2\sqrt{\omega}}{\sqrt{b_2\left(\kappa^2-8\right)}},\ a = -\frac{\omega}{\kappa^2-8},$$

where $b_2\left(\kappa^2-8\right) \neq 0$.

From the coefficients given above, we obtain the following combined periodic solution.

$$\Psi_{11}(x,t) = \left(\frac{\sqrt{\omega}\left(2-\sqrt{2}\csc(\zeta)\sec(\zeta)\right)}{\sqrt{b_2\left(\kappa^2-8\right)}}\right) \times e^{i\left(\theta_0+\frac{\Gamma(\beta+1)\left(\omega t^\alpha-\kappa x^\alpha\right)}{\alpha}\right)}. \quad (24)$$

Family-3: Setting $\vartheta_1 = \vartheta_2 = \vartheta_3 = \vartheta_4 = 1$ and $\tau_1 = \tau_2 = 0, \tau_3 = 1, \tau_4 = -1$, **Equation (17)** becomes

$$\Lambda(\zeta) = \mathrm{sech}(\zeta). \quad (25)$$

Substituting **Equations (18)** and **(25)** into **(3)**, we obtain a set of algebraic equations. Solving it, we obtain the following results:

Result-1:

$$\mu_0 = -\frac{\sqrt{\omega}}{\sqrt{b_2\left(-\left(\kappa^2+2\right)\right)}},\ \mu_1 = \frac{\sqrt{2}\sqrt{\omega}}{\sqrt{b_2\left(-\left(\kappa^2+2\right)\right)}},$$
$$\rho_1 = 0,\ b_1 = -\frac{3b_2\sqrt{\omega}}{\sqrt{b_2\left(-\left(\kappa^2+2\right)\right)}},\ a = -\frac{\omega}{\kappa^2+2},$$

where $b_2\left(\kappa^2+2\right) \neq 0$.

From the coefficients given above, we obtain the following bright soliton.

$$\Psi_{12}(x,t) = \left(\frac{\sqrt{\omega}\left(\sqrt{2}\mathrm{sech}(\zeta-1)\right)}{\sqrt{b_2\left(-\kappa^2-2\right)}}\right) \times e^{i\left(\theta_0+\frac{\Gamma(\beta+1)\left(\omega t^\alpha-\kappa x^\alpha\right)}{\alpha}\right)}. \quad (26)$$

Family-4: Setting $\vartheta_1 = 1-i, \vartheta_2 = 1+i, \vartheta_3 = \vartheta_4 = 1$ and $\tau_1 = i, \tau_2 = -i, \tau_3 = i, \tau_4 = -i$, **Equation (17)** becomes

$$\Lambda(\zeta) = \tan(\zeta) + 1. \quad (27)$$

Substituting **Equations (18)** and **(27)** into **(3)**, we obtain a set of nonlinear equations. Solving it, we obtain the following results:

Result-1:

$$\mu_0 = \frac{6\left(\sqrt{b_1^2\left(-\left(\kappa^2+4\right)^2\right)\omega^2} - b_1\left(\kappa^2+4\right)\omega\right)}{b_1^2\left(\kappa^2+4\right)^2},$$
$$\rho_1 = \frac{12\omega^2}{\sqrt{b_1^2\left(-\left(\kappa^2+4\right)^2\right)\omega^2}},\ b_2 = -\frac{b_1^2\left(\kappa^2+4\right)}{18\omega},$$
$$a = -\frac{\omega}{\kappa^2+4},\ \mu_1 = 0,$$

where $b_1\left(\kappa^2+4\right)\omega \neq 0$.

Using the coefficients determined in results-1, we yield the following mixed trigonometric solutions.

$$\Psi_{13}(x,t) = 6\omega\left(\frac{\omega(\cos(\zeta)-\sin(\zeta))}{\sqrt{b_1^2\left(-\left(\kappa^2+4\right)^2\right)\omega^2}(\sin(\zeta)+\cos(\zeta))} - \frac{1}{b_1\left(\kappa^2+4\right)}\right) \times e^{i\left(\theta_0+\frac{\Gamma(\beta+1)\left(\omega t^\alpha-\kappa x^\alpha\right)}{\alpha}\right)}. \quad (28)$$

Result-2:

$$\mu_0 = -\frac{6\omega}{\sqrt{b_1^2\left(-\left(\kappa^2+4\right)^2\right)}} - \frac{6\omega}{b_1\left(\kappa^2+4\right)},$$
$$\mu_1 = \frac{6\omega}{\sqrt{b_1^2\left(-\left(\kappa^2+4\right)^2\right)}},\ b_2 = -\frac{b_1^2\left(\kappa^2+4\right)}{18\omega},$$
$$a = -\frac{\omega}{\kappa^2+4},\ \rho_1 = 0,$$

where $b_1\left(\kappa^2+4\right),\ \omega \neq 0$.

Using the coefficients determined in Result-2, we obtain the following trigonometric solution.

$$\Psi_{14}(x,t)=\left(\frac{6\omega\tan(\zeta)}{\sqrt{b_1^2\left(-\left(\kappa^2+4\right)^2\right)}}-\frac{6\omega}{b_1\left(\kappa^2+4\right)}\right)\times e^{i\left(\theta_0+\frac{\Gamma(\beta+1)(\omega t^\alpha-\kappa x^\alpha)}{\alpha}\right)}. \tag{29}$$

Family-5: Setting $\vartheta_1=-3,\vartheta_2=-1,\vartheta_3=\vartheta_4=1$ and $\tau_1=1,\tau_2=-1,\tau_3=1,\tau_4=-1$, **Equation (17)** becomes

$$\Lambda(\zeta)=-\tanh(\zeta)-2. \tag{30}$$

Substituting **Equations (18)** and **(30)** into **(3)** yields a set of algebraic equations. Solving it, we obtain the following results:

Result-1:

$$\mu_0=\frac{18\omega}{b_1\left(\kappa^2-4\right)},\ \mu_1=0,\ \rho_1=\frac{18\omega}{b_1\left(\kappa^2-4\right)},$$
$$b_2=\frac{b_1^2\left(\kappa^2-4\right)}{18\omega},\ a=\frac{\omega}{4-\kappa^2},$$

where $b_1\left(\kappa^2-4\right),\omega\neq 0$.

Using the parameters obtained in Result-1, we obtain the following combined hyperbolic solution

$$\Psi_{15}(x,t)=\left(\frac{18\omega(\sinh(\zeta)+\cosh(\zeta))}{b_1(\kappa^2-4)(\sinh(\zeta)+2\cosh(\zeta))}\right)\times e^{i\left(\theta_0+\frac{\Gamma(\beta+1)(\omega t^\alpha-\kappa x^\alpha)}{\alpha}\right)}. \tag{31}$$

Result-2:

$$\mu_0=\frac{18\omega}{b_1\left(\kappa^2-4\right)},\ \mu_1=\frac{6\omega}{b_1\left(\kappa^2-4\right)},\ \rho_1=0,$$
$$b_2=\frac{b_1^2\left(\kappa^2-4\right)}{18\omega},\ a=\frac{\omega}{4-\kappa^2},$$

where $b_1\left(\kappa^2-4\right),\ \omega\neq 0$.

Using the parameters obtained in Result-2, we the following dark solution

$$\Psi_{16}(x,t)=\left(-\frac{6\omega(\tanh(\zeta-1))}{b_1\left(\kappa^2-4\right)}\right)\times e^{i\left(\theta_0+\frac{\Gamma(\beta+1)(\omega t^\alpha-\kappa x^\alpha)}{\alpha}\right)}. \tag{32}$$

Result-3:

$$\mu_0=\frac{48\omega}{b_1\left(\kappa^2-4\right)},\ \mu_1=\frac{12\omega}{b_1\left(\kappa^2-4\right)},\ \rho_1=\frac{36\omega}{b_1\left(\kappa^2-4\right)},$$
$$b_2=\frac{b_1^2\left(\kappa^2-4\right)}{72\omega},\ a=\frac{\omega}{4-\kappa^2},$$

where $b_1\left(\kappa^2-4\right),\ \omega\neq 0$.

Using the parameters calculated in Result-3, we obtain the following bright solution

$$\Psi_{17}(x,t)=\left(\frac{12\omega\mathrm{sech}^2(\zeta)}{b_1\left(\kappa^2-4\right)(\tanh(\zeta+2))}\right)\times e^{i\left(\theta_0+\frac{\Gamma(\beta+1)(\omega t^\alpha-\kappa x^\alpha)}{\alpha}\right)}. \tag{33}$$

Family-6: Setting $\vartheta_1=-1,\vartheta_2=0,\vartheta_3=\vartheta_4=1$ and $\tau_1=0,\tau_2=1,\tau_3=0,\tau_4=1$, **Equation (17)** becomes

$$\Lambda(\zeta)=-\frac{1}{e^\zeta+1}. \tag{34}$$

Substituting **Equations (34)** and **(18)** into **(3)**, we obtain a set of algebraic equations. Solving this system with Mathematica yields the following results.

Result-1:

$$\mu_0=\frac{\sqrt{2}\sqrt{\omega}}{\sqrt{b_2\left(\kappa^2-1\right)}},\ \mu_1=\frac{\sqrt{2}\sqrt{\omega}}{\sqrt{b_2\left(\kappa^2-1\right)}},\ \rho_1=0,$$
$$b_1=\frac{3b_2\sqrt{\omega}}{\sqrt{2}\sqrt{b_2\left(\kappa^2-1\right)}},\ a=-\frac{\omega}{\kappa^2-1},$$

where $b_2\left(\kappa^2-1\right)\neq 0$.

Result-2:

$$\mu_0=0,\ \mu_1=\frac{\sqrt{2}\sqrt{\omega}}{\sqrt{b_2\left(\kappa^2-1\right)}},\ \rho_1=0,$$
$$b_1=-\frac{3b_2\sqrt{\omega}}{\sqrt{2}\sqrt{b_2\left(\kappa^2-1\right)}},\ a=-\frac{\omega}{\kappa^2-1},$$

where $b_2\left(\kappa^2-1\right)\neq 0$.

Using the parameters calculated in Result-1 and Result-2, we obtain the following exponential solutions, respectively.

$$\Psi_{18}(x,t)=\left(\frac{\sqrt{2}\sqrt{\omega}e^{\frac{\Gamma(\beta+1)}{\alpha}(x^\alpha-\nu t^\alpha)}}{\sqrt{b_2(\kappa^2-1)}\left(e^{\frac{\Gamma(\beta+1)}{\alpha}(x^\alpha-\nu t^\alpha)}+1\right)}\right)\times e^{i\left(\theta_0+\frac{\Gamma(\beta+1)(\omega t^\alpha-\kappa x^\alpha)}{\alpha}\right)}. \tag{35}$$

$$\Psi_{19}(x,t)=\left(-\frac{\sqrt{2}\sqrt{\omega}}{\sqrt{b_2(\kappa^2-1)}\left(e^{\frac{\Gamma(\beta+1)}{\alpha}(x^\alpha-\nu t^\alpha)}+1\right)}\right)\times e^{i\left(\theta_0+\frac{\Gamma(\beta+1)(\omega t^\alpha-\kappa x^\alpha)}{\alpha}\right)}. \tag{36}$$

Family-7: Setting $\vartheta_1=-1,\vartheta_2=\vartheta_3=\vartheta_4=1$ and $\tau_1=1,\tau_2=-1,\tau_3=1,\tau_4=-1$, **Equation (17)** becomes

$$\Lambda(\zeta)=-\tanh(\zeta). \tag{37}$$

Substituting **Equations (37)** and **(18)** into **Equation (3)**, we obtain a system of algebraic equations. Solving it, we obtain the following results:

Result-1:

$$\mu_0 = \frac{2\sqrt{\omega}}{\sqrt{b_2\left(-\left(\kappa^2+8\right)\right)}},\ \mu_1 = -\frac{\sqrt{2}\sqrt{\omega}}{\sqrt{b_2\left(\kappa^2+8\right)}},$$
$$\rho_1 = \frac{\sqrt{2}\sqrt{\omega}}{\sqrt{b_2\left(\kappa^2+8\right)}},\ b_1 = \frac{6b_2\sqrt{\omega}}{\sqrt{b_2\left(-\left(\kappa^2+8\right)\right)}},\ a = -\frac{\omega}{\kappa^2+8},$$

where $b_2\left(\kappa^2+8\right) \neq 0$.

Using the coefficients from Result-1, we obtain the corresponding singular-dark soliton.

$$\begin{aligned}\Psi_{20}(x,t) &= \frac{\sqrt{\omega}}{\sqrt{-b_2^2\left(\kappa^2+8\right)^2}}\\ &\times\left(2\sqrt{b_2\left(\kappa^2+8\right)}\right.\\ &\left.-\sqrt{2}\sqrt{-b_2\left(\kappa^2+8\right)}\,\mathrm{csch}(\zeta)\,\mathrm{sech}(\zeta)\right)\\ &\times e^{i\left(\theta_0+\frac{\Gamma(\beta+1)\left(\omega t^\alpha-\kappa x^\alpha\right)}{\alpha}\right)}.\end{aligned} \tag{38}$$

Family-8: Setting $\vartheta_1 = 2-i, \vartheta_2 = 2+i, \vartheta_3 = \vartheta_4 = 1$ and $\tau_1 = i, \tau_2 = -i, \tau_3 = i, \tau_4 = -i$, **Equation (17)** becomes

$$\Lambda(\zeta) = \tan(\zeta) + 2. \tag{39}$$

Substituting **Equations (39)** and **(18)** into **Equation (3)**, yields a set of algebraic equations. Solving this system using Mathematica yields the following results.

Result-1:

$$\mu_0 = \frac{48\omega}{b_1\left(\kappa^2+4\right)},\ \mu_1 = -\frac{12\omega}{b_1\left(\kappa^2+4\right)},$$
$$\rho_1 = -\frac{60\omega}{b_1\left(\kappa^2+4\right)},\ b_2 = \frac{b_1^2\left(\kappa^2+4\right)}{72\omega},\ a = -\frac{\omega}{\kappa^2+4},$$

where $b_1\left(\kappa^2+4\right),\ \omega \neq 0$.

Using the coefficients from Result-1, we obtain the corresponding periodic solution.

$$\begin{aligned}\Psi_{21}(x,t) &= \left(-\frac{12\omega\sec^2(\zeta)}{b_1(\kappa^2+4)(\tan(\zeta)+2)}\right)\\ &\times e^{i\left(\theta_0+\frac{\Gamma(\beta+1)\left(\omega t^\alpha-\kappa x^\alpha\right)}{\alpha}\right)}.\end{aligned} \tag{40}$$

For all solutions $\zeta = \frac{\Gamma(\beta+1)}{\alpha}(x^\alpha - \nu t^\alpha)$.

Note: Under the transformation $\Psi = \Upsilon(\zeta)e^{i\Theta}$, the quadratic nonlinear term is $|\Psi|\Psi = |\Upsilon|\Upsilon e^{i\Theta}$. Therefore, the reduction $|\Upsilon|\Upsilon = \Upsilon^2$ is valid only on intervals where $\Upsilon(\zeta) \geq 0$. Accordingly, the reported solutions with $b_1 \neq 0$ are considered piecewise on their maximal regular intervals satisfying $\Upsilon \geq 0$, with all square-root arguments nonnegative and all denominators nonzero. For intervals where $\Upsilon < 0$, the relation $|\Upsilon|\Upsilon = -\Upsilon^2$ must be used instead. Thus, sign-changing and singular points are excluded from the stated domain of validity.

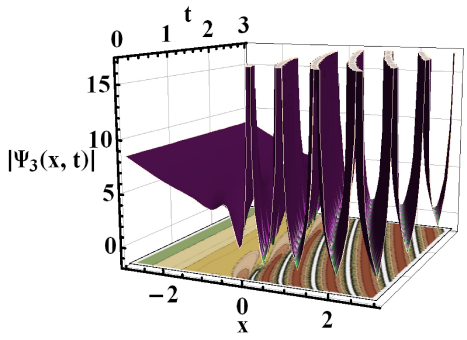
4. Graphical interpretation

The physical and graphical interpretation of some constructed solutions of the governing model emphasizes the considerable physical dynamics of 3D, and 2D representations, fractional effects, and temporal changes within the domain of soliton solutions and other scientific realms. These representations provide graphical insights into complex mathematical systems, helping investigators and scientists comprehend and analyze complex systems more effectively. The analyzed wave phenomena in this model have important applications in various fields, including nonlinear optics, communication systems, optical fibers, optical sensing, and many more. To ensure that the achieved results are not only clear but also physically meaningful graphical representations of the system have been drawn with utmost care using parameter values that emphasize important dynamics. For this reason, representative soliton solutions derived from the proposed methods are plotted to illustrate their dynamic behaviors, as depicted in **Figures 1**–**8**.

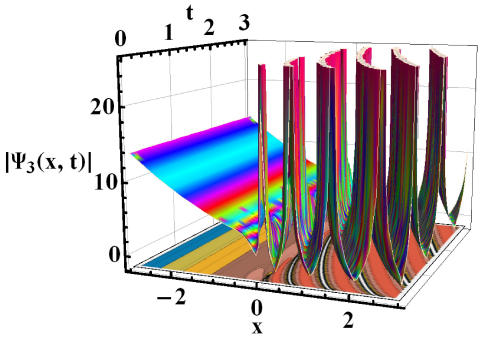
Figures 1 and **8** characterize the periodic solutions of **Equations (9)** and **(40)** with suitable parametric values $a = 0.5,\ b_2 = -1.4,\ \theta_0 = 0.05,\ \kappa = 0.7, \omega = 15.4$ and $a = -1.5,\ b_1 = 2.8,\ \theta_0 = 0.05,\ \kappa = 2.15,\ \omega = 0.3$, respectively. A periodic solution is a type of wave that repeats its configuration consistently over time or space.

Figures 2 and **5** represent the dark soliton solutions of **Equations (12)** and **(32)** with suitable parametric values $a = -0.9,\ b_2 = 0.5,\ \theta_0 = 0.08,\ \kappa = 0.05,\ \omega = 2$ and $a = -0.5,\ b_1 = 0.95,\ \theta_0 = 0.04,\ \kappa = 0.08,\ \omega = 2.6$, respectively. A dark soliton is a solution that exhibits lower intensity and propagates over a long distance, preserving its profile and speed. This property is central in nonlinear fiber optics, where dark solitons play a significant role in the dynamics of light pulses. Their inherent stability offers noteworthy potential for advancing fiber-optic communication systems, as they can minimize signal degradation over extended transmission distances.

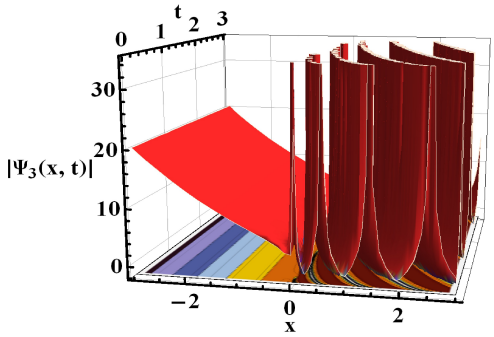
Figures 3 and **7** reveal the combined soliton structures of **Equations (22)** and **(38)** with suitable parametric values $a = -0.3,\ b_1 = 0.5,\ \theta_0 = 0.08,\ \kappa = 0.45,\ \omega = 0.7$ and $a = -0.25,\ b_2 = 0.68,\ \theta_0 = 0.02,\ \kappa = 0.25,\ \omega = 0.9$, respectively. The combined wave pattern is characterized by co-propagation with high intensity and discontinuity is known as a singular-bright soliton.



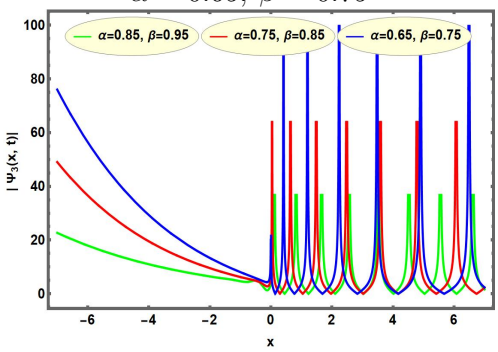
(a) Absolute behavior of $\Psi_3(x,t)$ at $\alpha = 0.85,\ \beta = 0.95$



(b) Absolute behavior of $\Psi_3(x,t)$ at $\alpha = 0.75,\ \beta = 0.85$



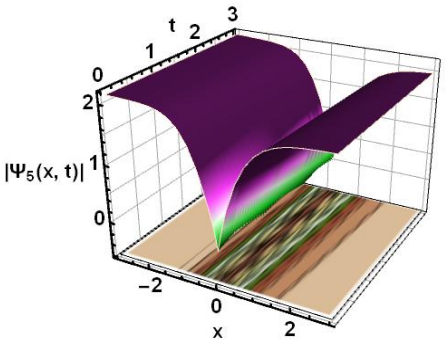
(c) Absolute behavior of $\Psi_3(x,t)$ at $\alpha = 0.65,\ \beta = 0.75$



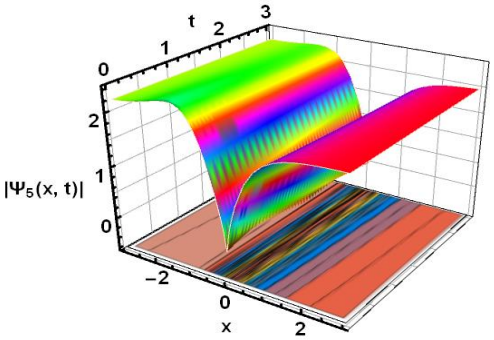
(d) Combined absolute behavior of $\Psi_3(x,t)$

Figure 1. Absolute graphical profiles of the solution $\Psi_3(x,t)$ with different parametric values of α and β

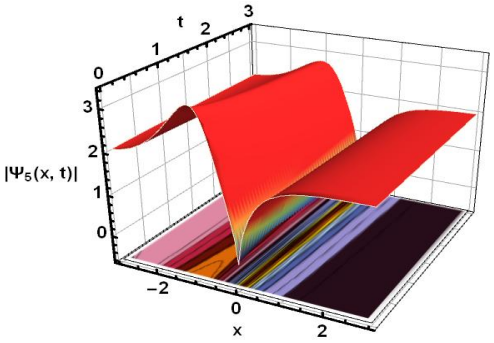
Figure 4 exhibits the bright soliton solutions of **Equation (26)** with appropriate parametric values $a = 0.095$, $b_2 = 0.085$, $\theta_0 = 0.03$, $\kappa = 0.017$, $\omega = 0.02$. A bright soliton is a solution that exhibits higher intensity. Bright solitons are vital to fiber-optic telecommunications, as their ability to propagate over long distances without distortion enables high-speed data transmission and reduces the need for signal regeneration.



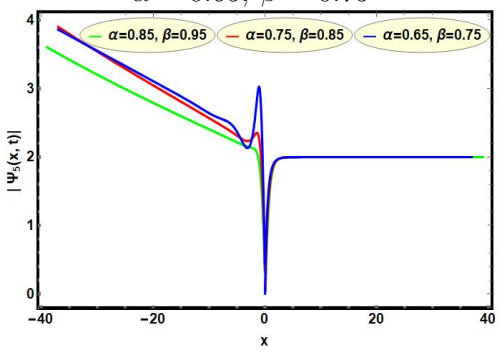
(a) Absolute behavior of $\Psi_5(x,t)$ at $\alpha = 0.85,\ \beta = 0.95$



(b) Absolute behavior of $\Psi_5(x,t)$ at $\alpha = 0.75,\ \beta = 0.85$



(c) Absolute behavior of $\Psi_5(x,t)$ at $\alpha = 0.65,\ \beta = 0.75$

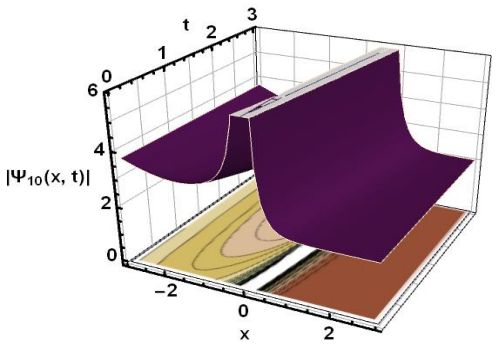


(d) Combined absolute behavior of $\Psi_5(x,t)$

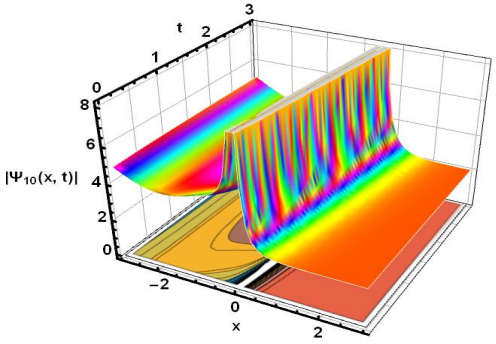
Figure 2. Absolute graphical profiles of the solution $\Psi_5(x,t)$ with different parametric values of α and β

Figure 6 shows the exponential solutions of **Equation (36)** with the appropriate parametric values $a = -0.3$, $b_2 = 0.1$, $\theta_0 = 0.03$, $\kappa = 0.17$, $\omega = 0.2$.

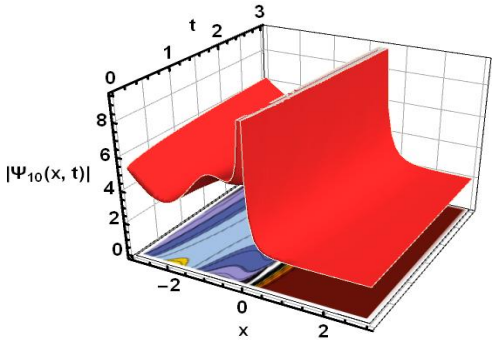
Parameters α and β describe the fractional behavior of the M-fractional derivative and define the degree of deviation from the integer-order derivatives. From a numerical point of view, different values of a, b_1, and b_2 influence the shape and size of the soliton profiles that we obtain, while the variation of α and β influences the propagation and dynamics of such solitons. Thus, increasing the dispersion coefficient broadens and shapes the pulse, while strong nonlinearities localize the pulse and increase its amplitude. These observations numerically illustrate the model's physical representation in terms of nonlinear pulse propagation and transmission through optical media, where the interplay of dispersion, nonlinearity, and fractional dynamics plays an important role in the dynamics of optical solitons. It should be worth mentioning that the solution families obtained using the GERFM method impose some compatibility conditions for the model parameters. Namely, the parameters of dispersion a and nonlinear interaction b_2 are not independent parameters for these solution families, since they can be calculated from the following algebraic equations including ω, κ, and b_1, subject to the corresponding nonzero-denominator conditions. These conditions arise naturally from the coefficient balancing process and delineate the allowed ranges of parameters for which the solutions are valid. Thus, the presented solutions should be viewed as valid within the restricted ranges of parameters and not as independent arbitrary choices of physical coefficients. The overall outcomes show that the fractional extended NLS equation has a remarkably wide range of dynamical phenomena, from stable soliton propagation to complex chaotic dynamics. The bifurcation analysis shows how the variation of physical parameters can cause qualitatively different wave dynamics, which can be very useful for the control and optimization of soliton-based optical systems. The chaotic analysis points out the fundamental limitations of long-term wave predictions and the importance of understanding the stability boundaries for applications in nonlinear optics.



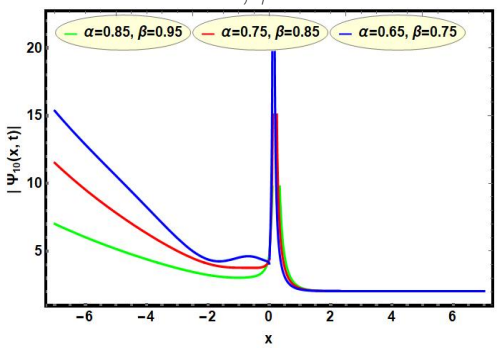
(a) Absolute behavior of $\Psi_{10}(x,t)$ at $\alpha = 0.85$, $\beta = 0.95$



(b) Absolute behavior of $\Psi_{10}(x,t)$ at $\alpha = 0.75$, $\beta = 0.85$

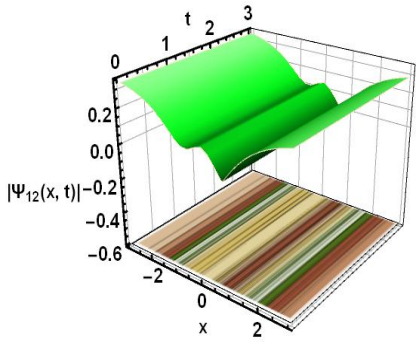


(c) Absolute behavior of $\Psi_{10}(x,t)$ at $\alpha = 0.65$, $\beta = 0.75$



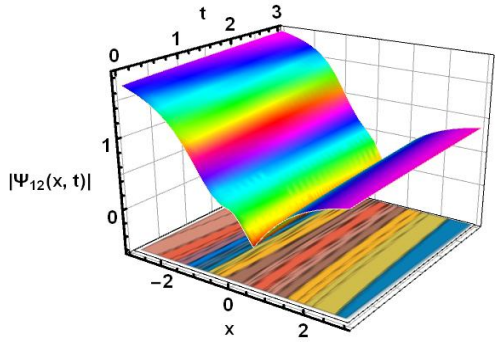
(d) Combined absolute behavior of $\Psi_{10}(x,t)$

Figure 3. Absolute graphical profiles of the solution $\Psi_{10}(x,t)$ with different parametric values of α and β

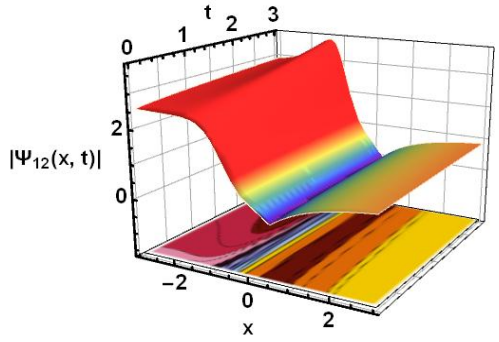


(a)

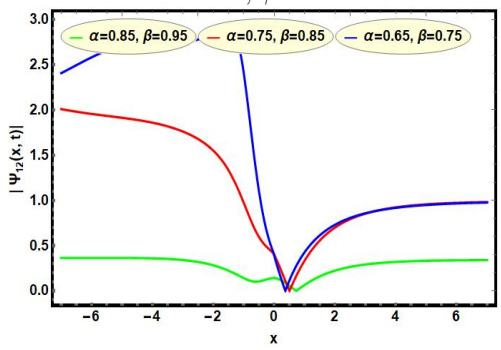
Absolute behavior of $\Psi_{12}(x,t)$ at $\alpha = 0.85,\ \beta = 0.95$



(b) Absolute behavior of $\Psi_{12}(x,t)$ at $\alpha = 0.75,\ \beta = 0.85$

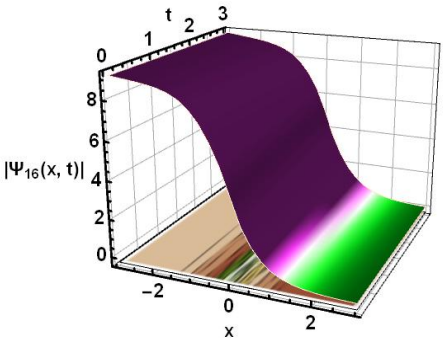


(c) Absolute behavior of $\Psi_{12}(x,t)$ at $\alpha = 0.65,\ \beta = 0.75$

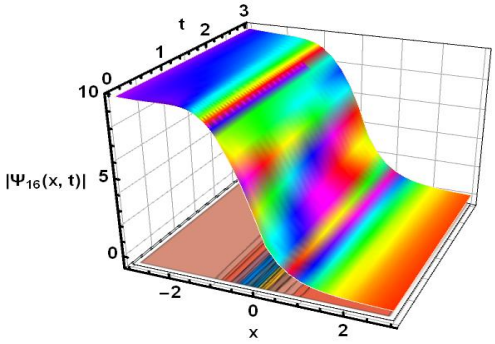


(d) Combined absolute behavior of $\Psi_{12}(x,t)$

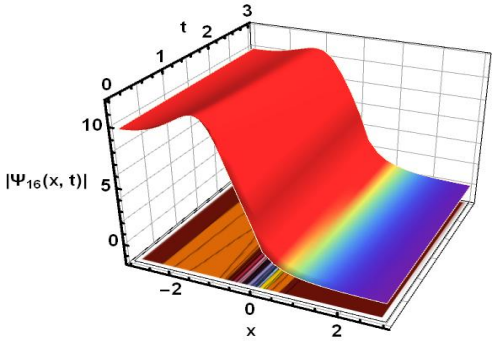
Figure 4. Absolute graphical profiles of the solution $\Psi_{12}(x,t)$ with different parametric values of α and β



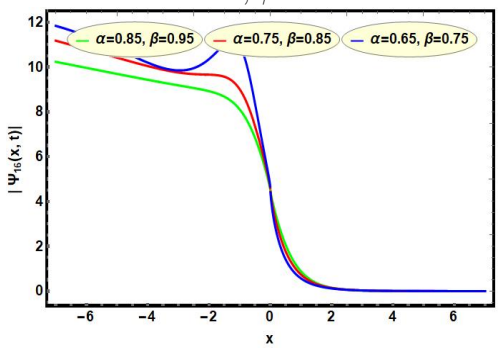
(a) Absolute behavior of $\Psi_{16}(x,t)$ at $\alpha = 0.85,\ \beta = 0.95$



(b) Absolute behavior of $\Psi_{16}(x,t)$ at $\alpha = 0.75,\ \beta = 0.85$

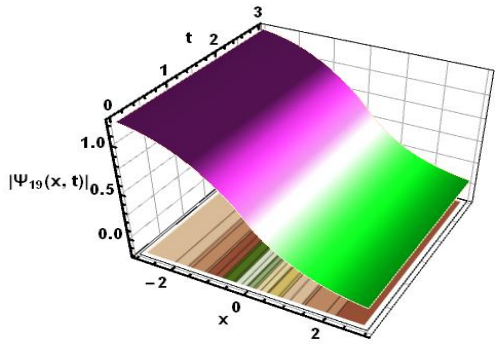


(c) Absolute behavior of $\Psi_{16}(x,t)$ at $\alpha = 0.65,\ \beta = 0.75$

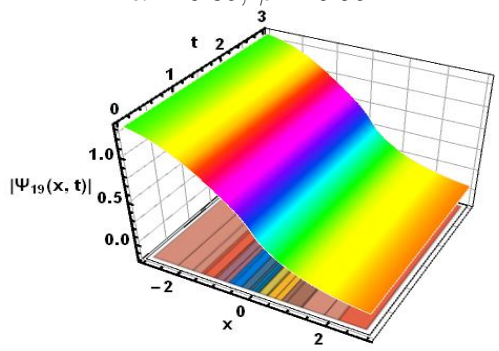


(d) Combined absolute behavior of $\Psi_{16}(x,t)$

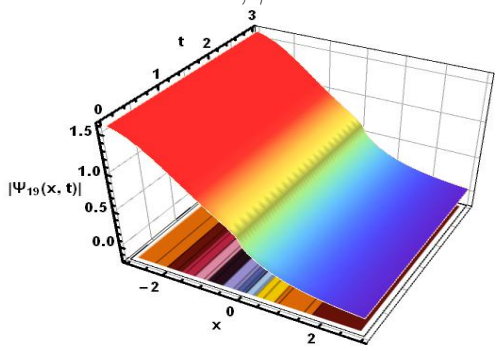
Figure 5. Absolute graphical profiles of the solution $\Psi_{16}(x,t)$ with different parametric values of α and β



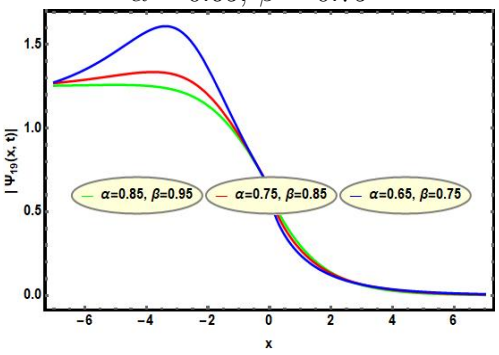
(a) Absolute behavior of $\Psi_{19}(x,t)$ at $\alpha = 0.85,\ \beta = 0.95$



(b) Absolute behavior of $\Psi_{19}(x,t)$ at $\alpha = 0.75,\ \beta = 0.85$



(c) Absolute behavior of $\Psi_{19}(x,t)$ at $\alpha = 0.65,\ \beta = 0.75$



(d) Combined absolute behavior of $\Psi_{19}(x,t)$

Figure 6. Absolute graphical profiles of the solution $\Psi_{19}(x,t)$ with different parametric values of α and β

5. Modulation instability analysis

In this section, we use linear stability analysis to investigate the MI of the fractional extended NLS equation with cubic-quadratic nonlinear terms. MI demonstrates an exponential increase of small perturbations in the amplitude or phase of a wave. Exploring MI is a critical phenomenon in nonlinear wave physics.[42] To study this phenomenon, we consider the M-fractional extended NLS equation with cubic-quadratic nonlinear terms and begin by assuming its stationary solution as:

$$\Psi(x,t) = a_0 e^{i\psi t^\alpha}, \tag{41}$$

where a_0 represents a real arbitrary constant. Substituting **Equation (41)** into **Equation (1)**, we get $\psi = \frac{(a_0^2 b_2 - a_0 b_1)\Gamma(\beta+1)}{\alpha}$. Assume the perturbed stationary solution is as follows:

$$\Psi(x,t) = (a_0 + \epsilon u(x,t)) e^{\frac{i((a_0^2 b_2 - a_0 b_1)\Gamma(\beta+1))t^\alpha}{\alpha}}, \tag{42}$$

where $u(x,t)$ indicates a fractional complex function whereas ϵ denotes a small, dimensionless perturbation parameter. Substituting **Equation (42)** into **Equation (1)** and linearizing the obtained result, we get

$$aD_{M,x}^{2\alpha,\beta} u + iD_{M,t}^{\alpha,\beta} u + \frac{1}{2}\left(2a_0^2 b_2 - a_0 b_1\right)(u + u^*) = 0. \tag{43}$$

Assume that **Equation (43)** has a solution of the form:

$$u(x,t) = \Omega_1 e^{i(mx^\alpha - wt^\alpha)} + \Omega_2 e^{-i(mx^\alpha - wt^\alpha)}, \tag{44}$$

where m indicates the wave number, w represents the frequency, and Ω_1, Ω_2 signify the coefficients of the linear combination. Substituting (44) into **Equation (43)**, we get the following system of equations:

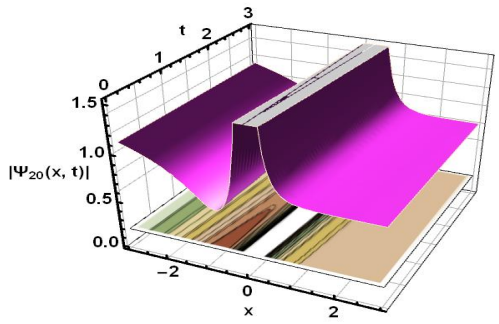
$$\begin{pmatrix} a_0^2 b_2 - \frac{a_0 b_1}{2} - \frac{a\alpha^2 m^2}{\Gamma(\beta+1)^2} + \frac{\alpha w}{\Gamma(\beta+1)} & a_0^2 b_2 - \frac{a_0 b_1}{2} \\ a_0^2 b_2 - \frac{a_0 b_1}{2} & a_0^2 b_2 - \frac{a_0 b_1}{2} - \frac{a\alpha^2 m^2}{\Gamma(\beta+1)^2} - \frac{\alpha w}{\Gamma(\beta+1)} \end{pmatrix} \begin{pmatrix} \Omega_1 \\ \Omega_2 \end{pmatrix} = \begin{pmatrix} 0 \\ 0 \end{pmatrix}, \tag{45}$$

Calculating the determinant and setting the result equal to zero, we obtain the following relationship:

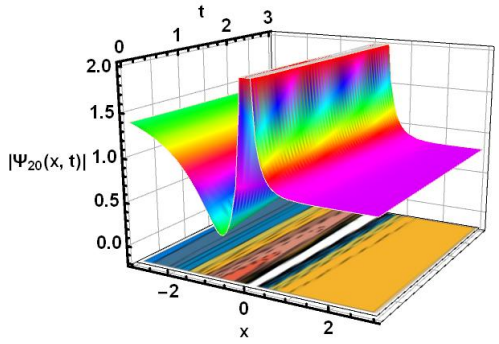
$$\frac{a^2\alpha^4 m^4}{\Gamma(\beta+1)^4} - \frac{\alpha^2\left(aa_0 m^2(2a_0 b_2 - b_1) + w^2\right)}{\Gamma(\beta+1)^2} = 0. \tag{46}$$

By taking into account **Equation (46)** , we can derive the following dispersion relation for **Equation (1)**:

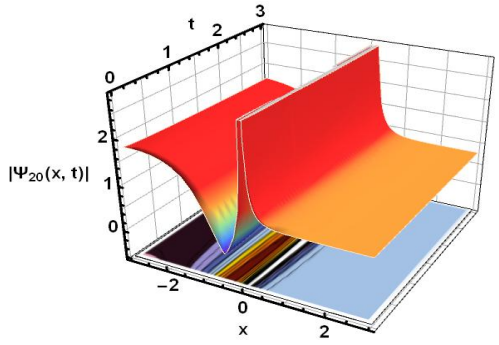
$$w = \left| \frac{\sqrt{a} m \sqrt{a_0\left(b_1 - 2a_0 b_2\right)\Gamma(\beta+1)^2 + a\alpha^2 m^2}}{\Gamma(\beta+1)} \right|. \tag{47}$$



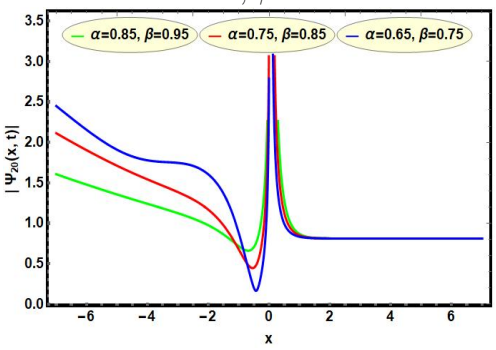
(a) Absolute behavior of $\Psi_{20}(x,t)$ at $\alpha = 0.85,\ \beta = 0.95$



(b) Absolute behavior of $\Psi_{20}(x,t)$ at $\alpha = 0.75,\ \beta = 0.85$

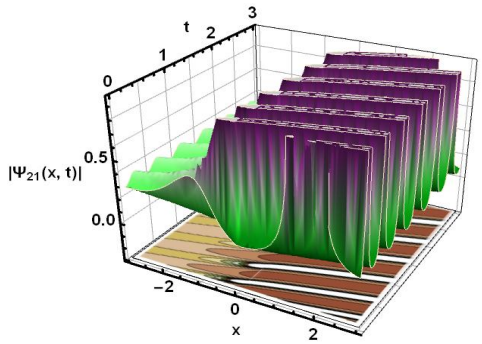


(c) Absolute behavior of $\Psi_{20}(x,t)$ at $\alpha = 0.65,\ \beta = 0.75$

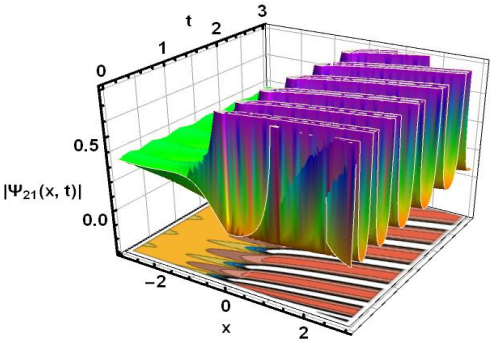


(d) Combined absolute behavior of $\Psi_{20}(x,t)$

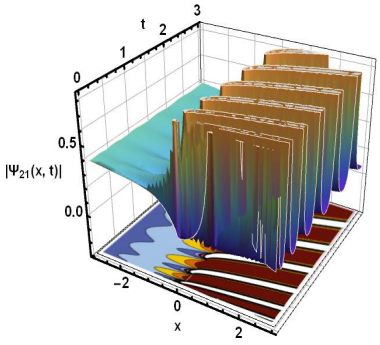
Figure 7. Absolute graphical profiles of the solution $\Psi_{20}(x,t)$ with different parametric values of α and β



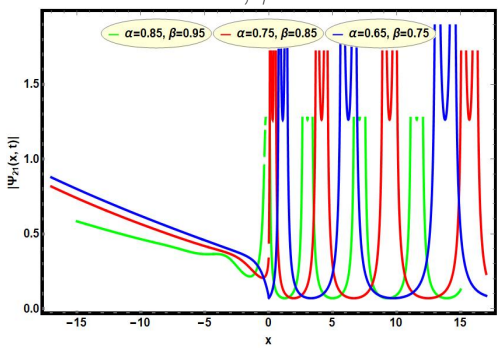
(a) Absolute behavior of $\Psi_{21}(x,t)$ at $\alpha = 0.85,\ \beta = 0.95$



(b) Absolute behavior of $\Psi_{21}(x,t)$ at $\alpha = 0.75,\ \beta = 0.85$



(c) Absolute behavior of $\Psi_{21}(x,t)$ at $\alpha = 0.65,\ \beta = 0.75$



(d) Combined absolute behavior of $\Psi_{21}(x,t)$

Figure 8. Absolute graphical profiles of the solution $\Psi_{21}(x,t)$ with different parametric values of α and β

From **Equation (47)**, we notice that the steady-state stability of **Equation (1)** arises when

$$a_0\left(b_1-2a_0b_2\right)\Gamma(\beta+1)^2+a\alpha^2m^2\geq 0. \quad (48)$$

The MI of **Equation (1)** occurs when the frequency w has an imaginary value, thus

$$a_0\left(b_1-2a_0b_2\right)\Gamma(\beta+1)^2+a\alpha^2m^2< 0. \quad (49)$$

In this context, the MI growth rate is expressed by the maximum absolute value of the imaginary part of the frequency, given as:

$$G(m)=2|\mathrm{Im}(w)|=$$
$$2\mathrm{Im}\left|\frac{\sqrt{a}m\sqrt{a_0\left(b_1-2a_0b_2\right)\Gamma(\beta+1)^2+a\alpha^2m^2}}{\Gamma(\beta+1)}\right|. \quad (50)$$

The incident power a_0 significantly affects the MI gain, as depicted in **Figure 9**.

Accordingly, the stability result must be interpreted as conditional: instability arises only within the finite gain bands shown in **Figure 9**, while the system remains stable for all parameter values outside these regions.

6. Sensitivity analysis

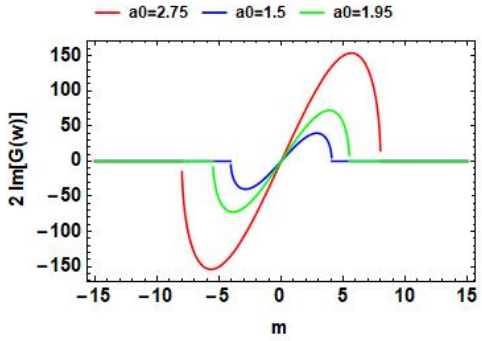
This section deals with sensitivity analysis of the studied fractional model. Sensitivity analysis examines the change in the dynamical behavior of a system in response to alterations in its initial conditions (ICs) or parameters. This analysis underlines the predictability and persistence of the system by detecting parameters or conditions that bring significant changes in behavior.[43,44] Therefore, this technique is valuable for locating the conditions that destabilize the system and for assessing its overall stability. We explore **Equation (3)** and convert it into a dynamical system.

$$\begin{aligned}\frac{d\Psi}{d\zeta}&=\Gamma(\zeta),\\ \frac{d\Gamma}{d\zeta}&=\lambda_1\Psi(\zeta)+\lambda_2\Psi^2(\zeta)-\lambda_3\Psi^3(\zeta),\end{aligned} \quad (51)$$

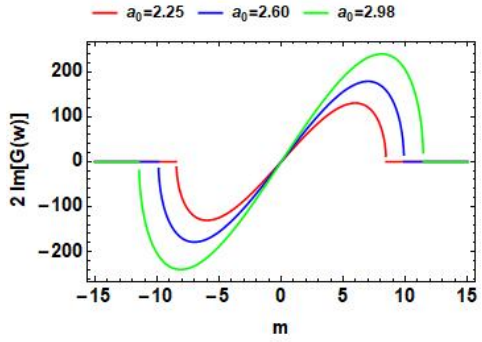
where $\lambda_1=\frac{a\kappa^2+\omega}{a}$, $\lambda_2=\frac{b_1}{a}$ and $\lambda_3=\frac{b_2}{a}$. The time-series solution curves are shown in **Figure 10** using specific parameter values: $\lambda_1=0.50, \lambda_2=0.10$ and $\lambda_3=0.01$.

The **Figure 10a** shows the trajectories of $\Psi(\zeta)$ for four sets of initial values, i.e., $(\Psi(0), \Gamma(0))$ = (0.01,0.01), (0.02,0.03), (0.03,0.04), and (0.04,0.05), marked by the blue solid, orange dashed, green dash-dotted, and red dotted curves. The solutions demonstrate repetitive positive peaks and negative troughs, with the magnitude and positions differing greatly depending on the initial conditions chosen.

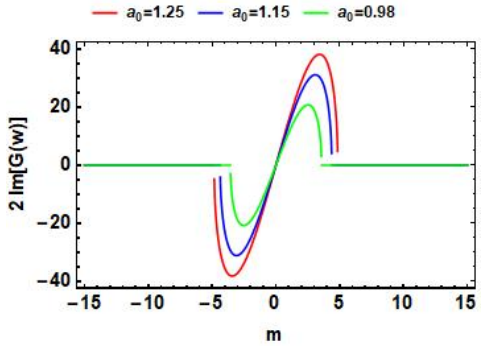
The trajectories of $\Gamma(\zeta)$ with the same initial conditions are depicted in **Figure 10b**. These solutions oscillate alternately positively and negatively and have clear extrema. The changes in the amplitudes and positions of the extrema with respect to small changes in the initial conditions indicate that the system dynamics is highly sensitive to the initial state. Thus, both figures clearly show the high dependence of the time behavior of the solutions on the initial conditions.



(a) $\alpha=1,\ \beta=1$



(b) $\alpha=0.70,\ \beta=0.75$



(c) $\alpha=0.60,\ \beta=0.50$

Figure 9. MI regions for different values of $a=2.4,\ b_1=4.34,\ b_2=5.87$

From the above diagrams, it can be noted that small variations in the initial conditions lead to significant differences in the system dynamics, indicating the complexity of the governing equation.

7. Bifurcation analysis

Bifurcation analysis is the study of the changes in the qualitative behavior of a system as a parameter varies. Such changes can cause equilibria, periodic orbits, or other system states to appear, disappear, or alter their stability. To analyze the bifurcation of the extended NLS equation, primarily in nonlinear systems, is a significant area of research due to its insightful applications for understanding intricate wave dynamics.[45,46] In this section, we use bifurcation theory to study the governing **Equation (1)**. By applying a Galilean transformation, **Equation (3)** can be reformulated as a planar dynamical system (PDS), facilitating a more comprehensive examination of its behavior.

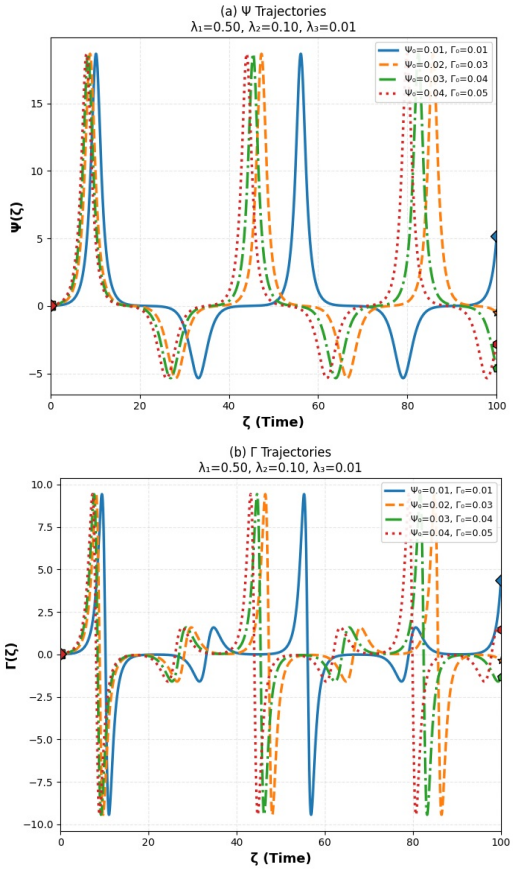


Figure 10. Sensitive analysis of the dynamical system (51) for $\lambda_1 = 0.50, \lambda_2 = 0.10$ and $\lambda_3 = 0.01$ at different initial values

$$\begin{aligned} \frac{d\Psi}{d\zeta} &= \Gamma(\zeta), \\ \frac{d\Gamma}{d\zeta} &= \lambda_1 \Psi(\zeta) + \lambda_2 \Psi^2(\zeta) - \lambda_3 \Psi^3(\zeta), \end{aligned} \tag{52}$$

where $\lambda_1 = \frac{a\kappa^2+\omega}{a}$, $\lambda_2 = \frac{b_1}{a}$ and $\lambda_3 = \frac{b_2}{a}$. The Hamiltonian function for **Equation (52)** is

$$\mathcal{H}(\Psi,\Gamma) = \frac{\Gamma^2}{2} - \lambda_1 \frac{\Psi^2}{2} - \lambda_2 \frac{\Psi^3}{3} + \lambda_3 \frac{\Psi^4}{4}. \tag{53}$$

Equation (52) has three equilibrium points, which are listed below:
$P_1 = (0,0)$, $P_2 = \left(\frac{\lambda_2 - \sqrt{\lambda_2^2+4\lambda_1\lambda_3}}{2\lambda_3}, 0\right)$, $P_3 = \left(\frac{\sqrt{\lambda_2^2+4\lambda_1\lambda_3}+\lambda_2}{2\lambda_3}, 0\right)$.

For **Equation (52)**, the Jacobian matrix determinant is

$$\begin{aligned} D(\Psi,\Gamma) &= \begin{vmatrix} 0 & 1 \\ \lambda_1 + 2\lambda_2\Psi^2 - 3\lambda_3\Psi^2 & 0 \end{vmatrix} \\ &= -\lambda_1 - 2\lambda_2\Psi + 3\lambda_3\Psi^2. \end{aligned} \tag{54}$$

From the theory of PDS, we have:

- The point (Ψ,Γ) is a saddle, if $D(\Psi,\Gamma) < 0$.
- The point (Ψ,Γ) is a center, if $D(\Psi,\Gamma) > 0$.
- The point (Ψ,Γ) is a cuspidal point, if $D(\Psi,\Gamma) = 0$.

The outcomes which may be obtained by changing the relevant parameters are described below.

Case-1: When $\lambda_1 > 0$, $\lambda_2 > 0$ and $\lambda_3 > 0$: By a suitable choice of parametric values for the parameters $a = 1$, $\kappa = 1$, $\omega = 1$, $b_1 = 1$, and $b_2 = 1$, we identify that $P_1 = (0,0), P_2 = (-1,0)$, and $P_3 = (2,0)$ are three equilibrium points in which P_1 behaves as a saddle whereas P_2 and P_3 behave as center points, as shown in **Figure 11**.

Case-2: When $\lambda_1 < 0$, $\lambda_2 < 0$ and $\lambda_3 < 0$: By setting the parameters $a = -1$, $\kappa = 2$, $\omega = 2$, $b_1 = 2$, and $b_2 = 1$, we examine that there are three equilibrium points $P_1 = (0,0), P_2 = (1+i,0)$, and $P_3 = (1-i,0)$. We observe that P_1 is the real equilibrium point as shown in **Figure 12**. Obviously, P_1 corresponds to the saddle point, where as the points P_2 and P_3 are imaginary points.

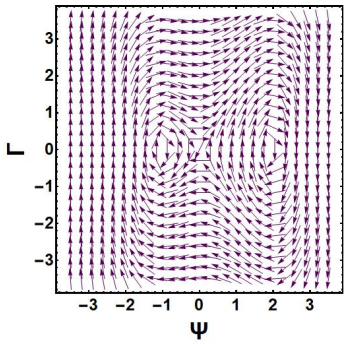
Case-3: When $\lambda_1 > 0$, $\lambda_2 < 0$ and $\lambda_3 > 0$: By taking the parameters $a = 1$, $\kappa = 1$, $\omega = 2$, $b_1 = -0.5$, and $b_2 = 1$, we identify that $P_1 = (0,0), P_2 = (-2,0)$, and $P_3 = (1.5,0)$ are three equilibrium points in which P_1 behaves as a saddle point whereas the points P_2 and P_3 behave as center points, as shown in **Figure 13**.

Case-4: When $\lambda_1 > 0$, $\lambda_2 > 0$ and $\lambda_3 < 0$: By selecting the parameters $a = 2$, $\kappa = 1.5$, $\omega = 1$, $b_1 = 3$, and $b_2 = -2$. We investigate that there are three equilibrium points $P_1 = (0,0)$, $P_2 = (-0.75 + 1.47902i, 0)$ and $P_3 = (-0.75 - 1.47902i, 0)$. The point P_1 is the only real equilibrium point, which is referred to as a saddle point and depicted in **Figure 14**. The remaining two points P_2 and P_3 are imaginary.

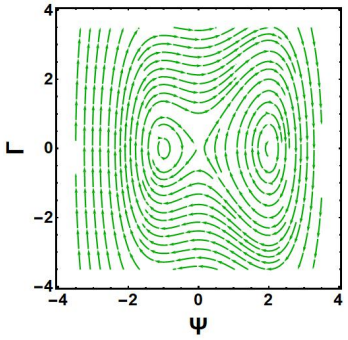
Case-5: When $\lambda_1 > 0$, $\lambda_2 < 0$ and $\lambda_3 < 0$: By picking the parameters $a = 1$, $\kappa = 2$, $\omega = 1$, $b_1 = -0.8$, and $b_2 = -0.5$. In this case, there are also three equilibrium points $P_1 = (0,0), P_2 =$

$(0.8 + 3.05941i, 0)$ and $P_3 = (0.8 - 3.05941i, 0)$. It is noted that P_1 is the only real equilibrium point, that serves as a saddle point and is depicted in **Figure 15**. The other two points P_2 and P_3 are imaginary points.

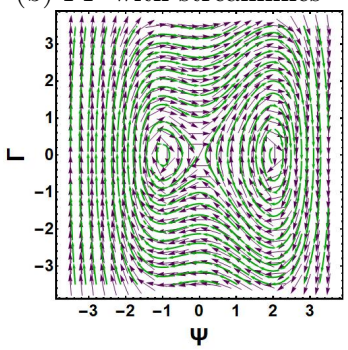
Case-6: When $\lambda_1 < 0$, $\lambda_2 > 0$ and $\lambda_3 > 0$: By choosing the parameters $a = 1$, $\kappa = 1$, $\omega = -3$, $b_1 = 1.5$, and $b_2 = 0.5$. In this case, there are also three equilibrium points $P_1 = (0, 0)$, $P_2 = (1.5 - 1.32288i, 0)$ and $P_3 = (1.5 + 1.32288i, 0)$. It is noted that P_1 is the only real equilibrium point that serves as the center point and is demonstrated in **Figure 16**. The other two points P_2 and P_3 are imaginary.



(a) PP with vector field

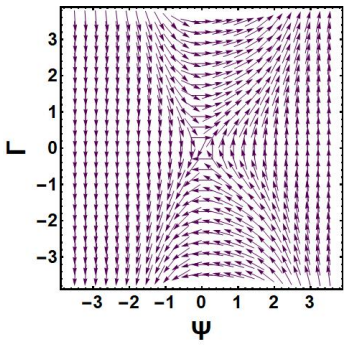


(b) PP with streamlines

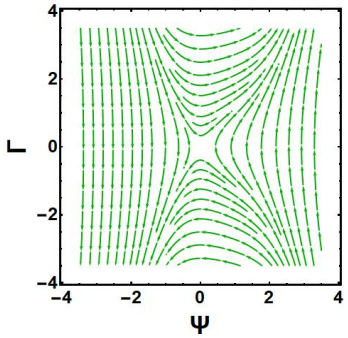


(c) PP with (a) and (b)

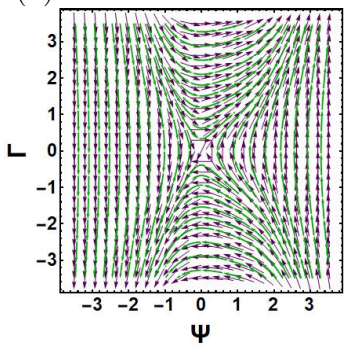
Figure 11. Dynamics of bifurcation when $\lambda_1 > 0$, $\lambda_2 > 0$ and $\lambda_3 > 0$



(a) PP with vector field



(b) PP with streamlines

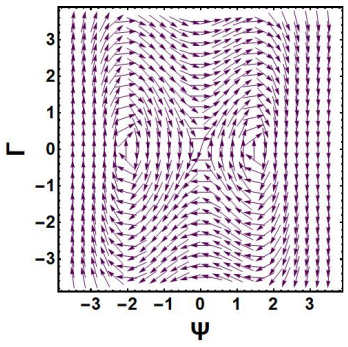


(c) PP with (a) and (b)

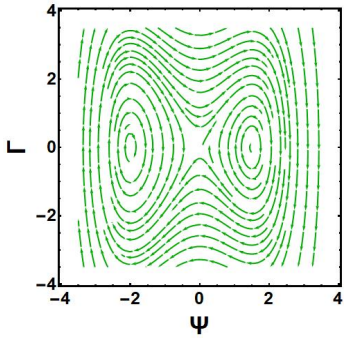
Figure 12. Dynamics of bifurcation when $\lambda_1 < 0$, $\lambda_2 < 0$ and $\lambda_3 < 0$

8. Chaos of the governing model

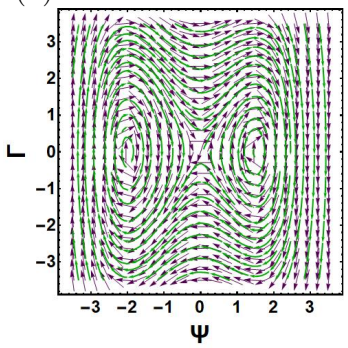
Chaotic analysis (CA) refers to the complex, unpredictable, and highly sensitive nature of a system's trajectories, often arising from the interplay between nonlinear dynamics and external disturbances. When assessing a perturbed dynamical system, determining how these disturbances affect its evolution is crucial. The system's reaction to perturbations is influenced by their specific features, making it necessary to employ advanced mathematical schemes such as nonlinear dynamics and chaos theory to explore and estimate its behavior effectively.[45,46] By introducing a perturbed term in the transformed dynamical system, the existence of CA is examined by observing time-series, two- and three-dimensional phase portraits.



(a) PP with vector field



(b) PP with streamlines



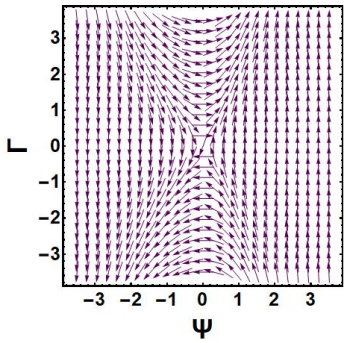
(c) PP with (a) and (b)

Figure 13. Dynamics of bifurcation when $\lambda_1 > 0$, $\lambda_2 < 0$ and $\lambda_3 > 0$

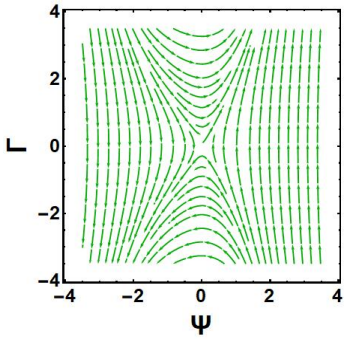
Consider the following dynamical system.

$$\begin{aligned} \frac{d\Psi}{d\zeta} &= \Gamma(\zeta), \\ \frac{d\Gamma}{d\zeta} &= \lambda_1 \Psi(\zeta) + \lambda_2 \Psi^2(\zeta) \\ &- \lambda_3 \Psi^3(\zeta) + \Omega \cos(\delta\zeta), \end{aligned} \tag{55}$$

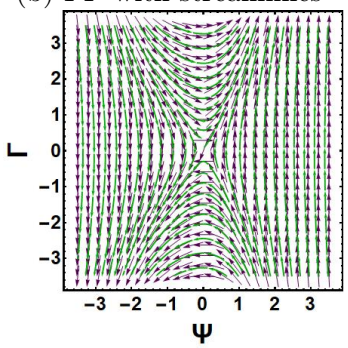
where $\lambda_1 = \frac{a\kappa^2+\omega}{a}$, $\lambda_2 = \frac{b_1}{a}$ and $\lambda_3 = \frac{b_2}{a}$, involving $\Omega\cos(\delta\zeta)$ as the perturbed term, where Ω and δ indicate the amplitude and frequency of the system, respectively. As illustrated in (17)–(19), the phase portraits exhibit remarkably rich and intricate behavior, underscoring a strong dependence on the parameter δ. The results reveal the dynamics of the system and its sensitivity to changes in the parameter δ, offering valuable insight into the influence of the perturbed term $\Omega\cos(\delta\zeta)$ on the system's behavior. These findings significantly contribute to a more comprehensive understanding of how small changes might alter the trajectories of the proposed dynamical system, eventually opening the door to more detailed and insightful predictions of its behaviors.



(a) PP with vector field



(b) PP with streamlines



(c) PP with (a) and (b)

Figure 14. Dynamics of bifurcation when $\lambda_1 > 0$, $\lambda_2 > 0$ and $\lambda_3 < 0$

8.1. Lyapunov exponent computation

This subsection discusses some steps to determine the Lyapunov exponent[47] of the dynamical system.

Step-1: Assume the following system is defined by

$$M_{j+1} = N(M_j), \tag{56}$$

where M_j stands for the state vector at the j-th iteration step, and N represents the system function.

Step-2: Select a point near the initial value of the curve M(0).

Step-3: Suppose that $M_j + \mu M_j$ is a neighbouring point with a small perturbation μM_j.
Step-4: By applying Taylor's theorem to the perturbation:

$$\mu M_{j+1} = \frac{\partial N}{\partial M}\,\mu M_j + \mathcal{O}(\|\mu M_j\|^2), \tag{57}$$

where the Jacobian matrix $\partial N/\partial M$ is evaluated along the reference trajectory at M_j.
Step-5: Assume

$$\lambda_j = \frac{1}{\Delta t}\ln\frac{\|\mu M_{j+1}\|}{\|\mu M_j\|}, \tag{58}$$

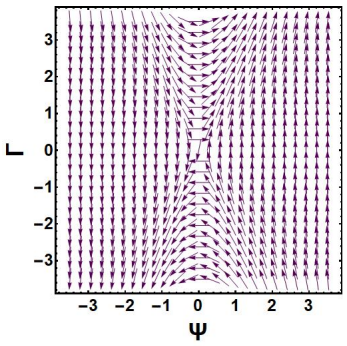
where λ_j is the local Lyapunov exponent at step j.
Step-6: To obtain the global Lyapunov exponent characterising the asymptotic behavior of the system, one performs a time average of the local exponents over a sufficiently large number of iterations:

$$\lambda = \lim_{n\to\infty}\frac{1}{n}\sum_{j=1}^{n}\lambda_j. \tag{59}$$

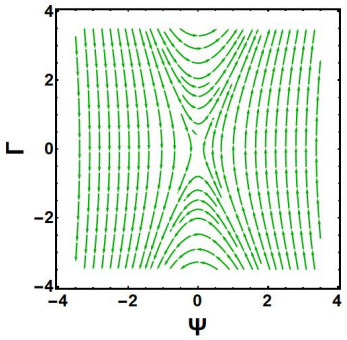
This above described method offers a quantitative criterion for identifying the point at which regular dynamics transit to chaotic dynamics, since a positive value of λ indicates sensitivity to initial conditions whereas a negative or zero value represents non-chaotic behavior.

Figure 17a shows the three-dimensional trajectory in the (ζ, Ψ, Γ) space. The orbit remains bounded but does not repeat along a simple closed path. Its irregular oscillations indicate complicated long-time dynamics. **Figure 17b** presents the corresponding phase portrait in the (Ψ, Γ) plane. The trajectories form a stretched and folded two-lobed structure, rather than a single closed orbit, indicating strong sensitivity in the state-space evolution. **Figure 17c** gives the Poincaré section obtained by sampling the trajectory at the forcing period. The points are spread over a finite region instead of concentrating on a few points or a smooth closed curve, which is consistent with a chaotic response. **Figure 17d** shows the evolution of the Lyapunov exponents. After the initial transient, the largest exponent approaches approximately $L_1 = 0.0698$, while the second exponent approaches $L_2 = -0.0698$, with the forcing-related exponent close to zero. The positive largest exponent provides quantitative evidence of sensitive dependence on initial conditions.

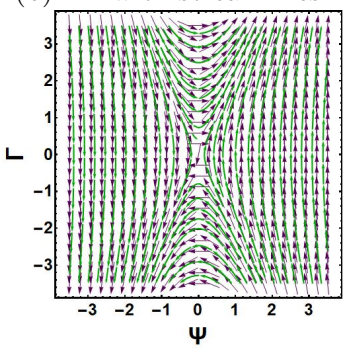
Figure 18a shows a bounded but more irregular three-dimensional trajectory than that observed for $\delta = 1.20$. **Figure 18b** displays the phase portrait, where the trajectories form a dense folded structure around the two principal regions of motion. **Figure 18c** shows a dispersed Poincaré section covering a relatively broad area of the phase plane. The absence of a finite collection of isolated points indicates that the response is not simply periodic. **Figure18d** gives the Lyapunov-exponent evolution, with the largest exponent approaching $L_1 \approx 0.2502$ and the second exponent approaching $L_2 \approx -0.2502$, while the remaining exponent is approximately zero. The increase in L_1 from 0.0698 to 0.2502 indicates stronger sensitivity to initial conditions at the higher forcing frequency.



(a) PP with vector field



(b) PP with streamlines

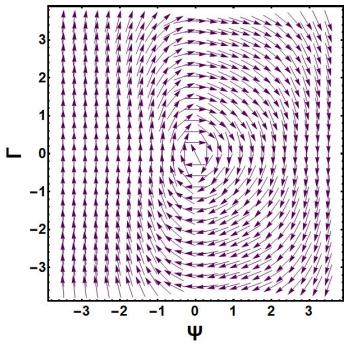


(c) PP with (a) and (b)

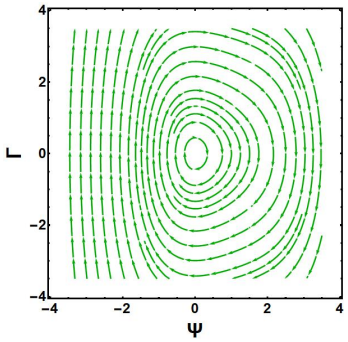
Figure 15. Dynamics of bifurcation when $\lambda_1 > 0$, $\lambda_2 < 0$ and $\lambda_3 < 0$

Figure 19a illustrates the bounded three-dimensional trajectory for $\delta = 2.0$. The orbit continues to oscillate irregularly without approaching a simple periodic path. **Figure 19b** shows a well-developed folded structure in the (Ψ, Γ) plane,

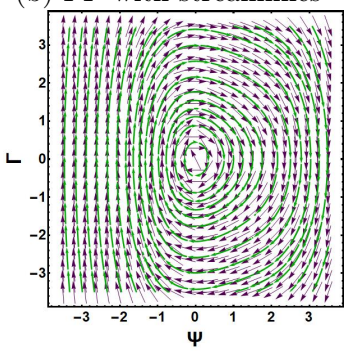
indicating repeated stretching and contraction of neighboring trajectories. **Figure 19c** contains a broad distribution of Poincaré points, providing further evidence that the motion is aperiodic and dynamically complex. **Figure 19d** shows that the Lyapunov exponents settle to approximately $L_1 = 0.1414$ and $L_2 = -0.1414$, together with a zero exponent associated with the periodically forced formulation. Since L_1 remains positive, the system retains chaotic behavior, although the degree of sensitivity is lower than that observed for $\delta = 1.90$.



(a) PP with vector field



(b) PP with streamlines



(c) PP with (a) and (b)

Figure 16. Dynamics of bifurcation when $\lambda_1 < 0$, $\lambda_2 > 0$ and $\lambda_3 > 0$

Physical justification: The chaos is generated by the interplay of the nonlinear term with the periodic perturbation $\Omega\cos(\delta\zeta)$. The balance between them generates an irregular oscillation and modifies the trajectory structure as the forcing parameter δ is varied. **Quantitative rigor**: Identification of chaos is based on the largest Lyapunov exponent and the Poincaré sections. The positive values of the largest Lyapunov exponents $L_{\max} = 0.0698$, 0.2502, and 0.1414 for $\delta = 1.20$, 1.90, and 2.0, respectively, prove that there is an exponential divergence of neighboring trajectories. The largest value at $\delta = 1.90$ indicates the strongest sensitivity to initial conditions, while the scattered Poincaré points provide independent support for the chaotic dynamics.

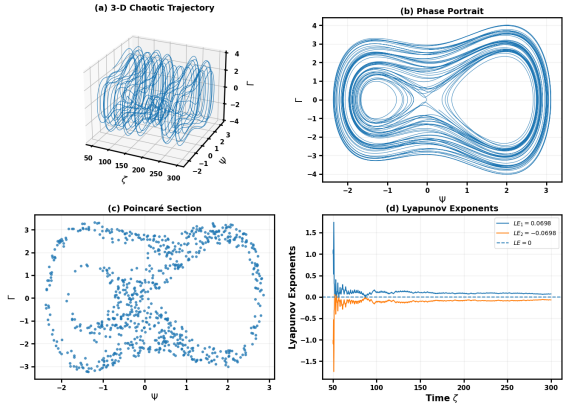


Figure 17. CA for system (55) when $a = 0.3$, $\omega = 0.2$, $\kappa = 1.5$, $b_1 = 0.25, b_2 = 0.35, \Omega = 0.3$, and $\delta = 1.20$ using $\Psi(0) = 0.20, \Gamma(0) = 0.15$

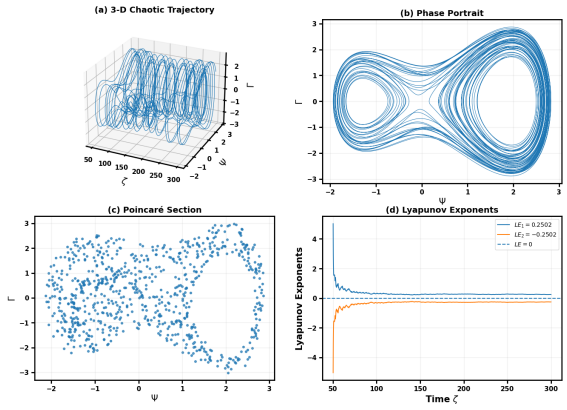


Figure 18. CA for system (55) when $a = 0.3$, $\omega = 0.2$, $\kappa = 1.5$, $b_1 = 0.25, b_2 = 0.35, \Omega = 0.3$, and $\delta = 1.90$ using $\Psi(0) = 0.20, \Gamma(0) = 0.15$

9. Comparison and novelty

In this section, we concisely compare our extracted results in the form of bright solutions, periodic solitons, dark solitons, and other wave structures with the results obtained by the investigators in.[27] The novelty of the current study is discussed in **Table 1**.

The novelty of the paper is not only due to the use of well-known analytical methods. The major novelty of this research is the detailed analysis of the M-fractional extended NLS equation,

which is a generalized framework for investigating the dynamics of nonlinear waves and their corresponding nonlinear behavior. Using ERSC–SHC and GERFM approaches, we find several families of exact soliton solutions; at the same time, using modulation instability, sensitivity, bifurcation and chaos analysis, we obtain additional information regarding the stability of exact solutions, their dependence on parameters, and the transition from regular to complicated dynamics. In contrast to earlier research, where only exact solutions of fractional NLS-type models were derived, our research demonstrates the link between the exact solution of the wave equation and the nonlinear behavior of the corresponding nonlinear system.

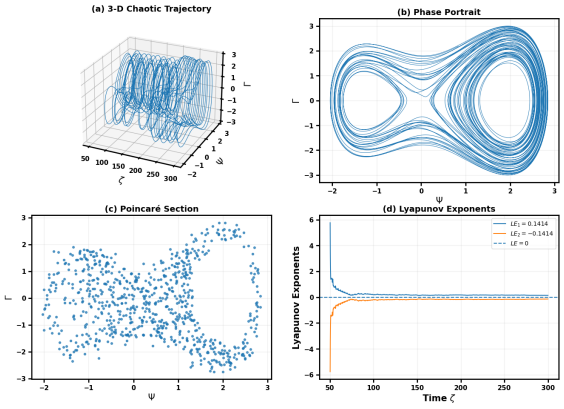


Figure 19. CA for system (55) when $a = 0.3$, $\omega = 0.2$, $\kappa = 1.5$, $b_1 = 0.25, b_2 = 0.35, \Omega = 0.3$, and $\delta = 2$ using $\Psi(0) = 0.20, \Gamma(0) = 0.15$

Table 1. Comparison of the previous study[27] with the present study

Features / Analysis	**Previous study[27]**	**Present study**
Governing model	Extended NLS equation	M-fractional extended NLS equation
Fractional formulation	Not considered	M-truncated fractional derivative
Nonlinear terms	Cubic-quadratic nonlinear terms	Cubic-quadratic nonlinear terms
Analytical method	Method of undetermined coefficients	ERSC–SHC and GERFM
Bright soliton solutions	✓	✓
Dark soliton solutions	✓	✓
Singular soliton solutions	✓	✓
Exponential solutions	×	✓
Combined soliton structures	Limited	✓
Modulation instability (MI)	×	✓
Sensitivity analysis	×	✓
Bifurcation analysis	×	✓
Chaos analysis	×	✓
Phase portraits	Not investigated	✓
Graphical visualization	Limited	✓
Qualitative analysis	×	✓
Overall scope	Exact solutions and conservation laws	Exact solutions, MI, sensitivity, bifurcation, and chaos

10. Conclusion

This investigation has explored the diverse range of soliton solutions of the M-fractional extended NLS equation incorporating cubic-quadratic nonlinearity. A rich spectrum of distinct soliton solutions in the form of bright, dark, singular, periodic, and exponential were revealed by employing two methodologies. These derived solutions are of substantial importance and have significant potential in transmission and telecommunications systems because they sustain their shape and velocity while propagating through a medium. The constructed solutions were also validated using Mathematica, which reflects the efficiency and correctness of the applied methodologies. The MI of the fractional model was also explored through linear stability theory. Moreover, to enhance our understanding of the underlying PDS, we also performed a comprehensive qualitative analysis of the governing problem, which showed how slight parameter variations can cause substantial behavioral shifts, leading to transitions from stable states to chaotic regimes. The graphical depictions in the form of 2D and 3D provided profound understanding into the dynamic features and evolution of the solitons, allowing for a deeper insight of how parameters and fractional-order effects affects the shape of the wave form structures. The results obtained in this study have practical applications in the modern telecommunications industry, where continuous advancements over the

past few decades have led to remarkable innovations in telecom systems, internet technologies, and social media platforms, thereby transforming global communication. In the future, the governing model can be extended to include additional forms of nonlinearity, as well as stochastic and alternative fractional operators, potentially uncovering new categories of soliton solutions and broadening the model's applicability to a wider range of physical systems.

Acknowledgments

This research was funded by King Mongkut's University of Technology North Bangkok, Contract No. KMUTNB-69-KNOW-47. In addition, the first author was financially supported by King Mongkut's University of Technology North Bangkok under contract no. KMUTNB-Post-69-02.

Funding

This research was funded by King Mongkut's University of Technology North Bangkok, Contract No. KMUTNB-69-KNOW-47. In addition, the first author was financially supported by King Mongkut's University of Technology North Bangkok under contract no. KMUTNB-Post-69-02.

Conflict of interest

The authors declare they have no competing interests.

Author contributions

Conceptualization: All authors
Data curation: All authors
Formal analysis: Shafqat Ur Rehman, Sekson Sirisubtawee
Funding acquisition: Sekson Sirisubtawee
Investigation: All authors
Methodology: All authors
Project administration: Sekson Sirisubtawee
Resources: Sekson Sirisubtawee
Software: Shafqat Ur Rehman, Sekson Sirisubtawee
Supervision: Sekson Sirisubtawee
Visualization: All authors
Validation: All authors
Writing–original draft: Shafqat Ur Rehman, Sekson Sirisubtawee
Writing–review & editing: All authors

Availability of data

Not applicable.

AI tools statement

All authors confirm that no AI tools were used in the preparation of this manuscript.

References

1. Mohan B, Kumar S. Generalization and analytic exploration of soliton solutions for nonlinear evolution equations via a novel symbolic approach in fluids and nonlinear sciences. *Chin J Phys.* 2024;92:10-21. https://doi.org/10.1016/j.cjph.2024.09.004
2. Sagib M, Saha BK, Mohanty SK, Rahman MS. Diverse soliton solutions to the nonlinear partial differential equations related to electrical transmission line. *Phys Scr.* 2024;99(9):095219. https://doi.org/10.1088/1402-4896/ad69e6
3. Wang KL. New dynamical behaviors and soliton solutions of the coupled nonlinear Schrödinger equation. *Int J Geom Methods Mod Phys.* 2025;22(8):2550047. https://doi.org/10.1142/S0219887825500471
4. Bilal M, Rehman SU, Alawaideh YM, Popa IL, Al-khamiseh BM. On the study of multiple wave profiles and hybrid phenomena to the newly developed multi-component Gross-Pitaevskii system and stability analysis. *Ain Shams Eng J.* 2025;16(9):103510. https://doi.org/10.1016/j.asej.2025.103510
5. Khan MAU, Sadaf M, Akram G, Birhanu A, Rehan K, Hamed YS. Soliton solutions of nonlinear coupled Davey-Stewartson Fokas system using modified auxiliary equation method and extended $(\frac{G'}{G^2})$-expansion method. *Sci Rep.* 2024;14(1):21949. https://doi.org/10.1038/s41598-024-72571-0
6. Rehman SU, Ahmad J. Stability analysis and novel optical pulses to Kundu-Mukherjee-Naskar model in birefringent fibers. *Int J Mod Phys B.* 2024;38(15):2450192. https://doi.org/10.1142/S0217979224501923
7. Sulaiman TA, Bulut H. The new extended rational SGEEM for construction of optical solitons to the (2+1)-dimensional Kundu-Mukherjee-Naskar model. *Appl Math Nonlinear Sci.* 2019;4(2):513-522. https://doi.org/10.2478/AMNS.2019.2.00048
8. Zhang J, Manafian J, Raut S, Roy S, Mahmoud KH, Alsubaie ASA. Study of two soliton and shock wave structures by weighted residual method and Hirota bilinear approach. *Nonlinear Dyn.* 2024;112(14):12375-12391. https://doi.org/10.1007/s11071-024-09706-5
9. Tipu GH, Faridi WA, Myrzakulova Z, Myrzakulov R, AlQahtani SA, AlQahtani NF, *et al.* On optical soliton wave solutions of non-linear Kairat-X equation via new extended direct algebraic method. *Opt Quantum Electron.* 2024;56(4):655. https://doi.org/10.1007/s11082-024-06369-9

10. Wang SF. Dromion solutions of nonlinear BKK equations using the improved F-expansion method. *Pramana J Phys.* 2025;99(2):60. https://doi.org/10.1007/s12043-025-02915-6
11. Batool S, Arshad M, Perveen N, Sarwar S. Bright optical solution for fractional Lakshmanan-Porsezian-Daniel with spatio temporal dispersion by improved Adomian decomposition method. *Opt Quantum Electron.* 2024;56(7):1137. https://doi.org/10.1007/s11082-024-07048-5
12. Zayed EME, Alurrfi KAE. The $(\frac{G'}{G}, \frac{1}{G})$-expansion method and its applications to two nonlinear Schrödinger equations describing the propagation of femtosecond pulses in nonlinear optical fibers. *Optik.* 2016;127(4):1581-1589. https://doi.org/10.1016/j.ijleo.2015.11.027
13. Tahir M, Awan AU, Abro KA. Extraction of optical solitons in birefringent fibers for Biswas-Arshed equation via extended trial equation method. *Nonlinear Eng.* 2021;10(1):146-158. https://doi.org/10.1515/nleng-2021-0011
14. Ozisik M, Secer A, Bayram M. On the investigation of chiral solitons via modified new Kudryashov method. *Int J Geom Methods Mod Phys.* 2023;20(07):2350117. https://doi.org/10.1142/S0219887823501177
15. Sabi'u J, Ibrahim IS, Neamprem K, Sungnul S, Sirisubtawee S. Generalized modified unstable nonlinear Schrödinger's equation: Optical solitons and modulation instability. *Mathematics.* 2025;13(12):2032. https://doi.org/10.3390/math13122032
16. Bilal M, Ren J, Alsubaie ASA, Mahmoud KH, Inc M. Dynamics of nonlinear diverse wave propagation to improved Boussinesq model in weakly dispersive medium of shallow waters or ion acoustic waves using efficient technique. *Opt Quantum Electron.* 2024;56(1):21. https://doi.org/10.1007/s11082-023-05587-x
17. Hussain E, Malik S, Yadav A, Shah SAA, Iqbal MAB, Ragab AE, *et al.* Qualitative analysis and soliton solutions of nonlinear extended quantum Zakharov-Kuznetsov equation. *Nonlinear Dyn.* 2024;112(21):19295-19310. https://doi.org/10.1007/s11071-024-09992-z
18. Younis M, Bilal M, Rehman SU, Seadawy AR, Rizvi STR. Perturbed optical solitons with conformable time-space fractional Gerdjikov-Ivanov equation. *Math Sci.* 2022;16(4):431-443. https://doi.org/10.1007/s40096-021-00431-3
19. Younas T, Ahmad J. Novel soliton insights into generalized fractional Tzitzéica-type evolution equations using the modified Khater method. *Mod Phys Lett B.* 2025;39(10):2450441. https://doi.org/10.1142/S0217984924504414
20. Lan ZZ. Multi-soliton solutions, breather-like and bound-state solitons for complex modified Korteweg-de Vries equation in optical fibers. *Chin Phys B.* 2024;33(6):060201. https://doi.org/10.1088/1674-1056/ad39d7
21. Kumar S, Kukkar A. Dynamics of several optical soliton solutions of a (3+1)-dimensional nonlinear Schrödinger equation with parabolic law in optical fibers. *Mod Phys Lett B.* 2025;39(09):2450453. https://doi.org/10.1142/S0217984924504530
22. Asghari Y, Eslami M, Matinfar M, Rezazadeh H. Novel soliton solution of discrete nonlinear Schrödinger system in nonlinear optical fiber. *Alex Eng J.* 2024;90:7-16. https://doi.org/10.1016/j.aej.2024.01.024
23. Akram S, Ahmad J, Rehman SU. Stability analysis and dynamical behavior of solitons in nonlinear optics modelled by Lakshmanan-Porsezian-Daniel equation. *Opt Quantum Electron.* 2023;55(8):685. https://doi.org/10.1007/s11082-023-04986-4
24. Das A, Karmakar B, Biswas A, Yıldırım Y, Alghamdi AA. Chirped periodic waves and solitary waves for a generalized derivative resonant nonlinear Schrödinger equation with cubic-quintic nonlinearity. *Nonlinear Dyn.* 2023;111(16):15347-15371. https://doi.org/10.1007/s11071-023-08640-2
25. Abdullaev FK, Gammal A, Tomio L, Frederico T. Stability of trapped Bose-Einstein condensates. *Phys Rev A.* 2001;63(4):043604. https://doi.org/10.1103/PhysRevA.63.043604
26. Benney DJ, Newell AC. The propagation of nonlinear wave envelopes. *J Math Phys.* 1967;46(1-4):133-139. https://doi.org/10.1002/sapm1967461133
27. Triki H, Biswas A, Moshokoa SP, Belic M. Optical solitons and conservation laws with quadratic-cubic nonlinearity. *Optik.* 2017;128:63-70. https://doi.org/10.1016/j.ijleo.2016.10.010
28. Pal R, Loomba S, Kumar CN. Chirped self-similar waves for quadratic-cubic nonlinear Schrödinger equation. *Ann Phys.* 2017;387:213-221. https://doi.org/10.1016/j.aop.2017.10.007
29. Fujioka J, Cortés E, Pérez-Pascual R, Rodríguez RF, Espinosa A, Malomed BA. Chaotic solitons in the quadratic-cubic nonlinear Schrödinger equation under nonlinearity management. *Chaos.* 2011;21(3):033120. https://doi.org/10.1063/1.3629985
30. Biswas A, Ullah MZ, Asma M, Zhou Q, Moshokoa SP, Belic M. Optical solitons with quadratic-cubic nonlinearity by semi-inverse variational principle. *Optik.* 2017;139:16-19. https://doi.org/10.1016/j.ijleo.2017.03.111
31. Aslan EC, Inc M. Soliton solutions of NLSE with quadratic-cubic nonlinearity and stability analysis. *Waves Random Complex Media.* 2017;27(4):594-601. https://doi.org/10.1080/17455030.2017.1286060
32. Inc M, Aliyu AI, Yusuf A, Baleanu D. Optical solitons and modulation instability analysis to the quadratic-cubic nonlinear Schrödinger equation. *Nonlinear Anal Model Control.* 2019;24(1):20-33. https://doi.org/10.15388/NA.2019.1.2

33. Attia RA, Khater M, El-Sayed Ahmed A, El-Shorbagy MA. Accurate sets of solitary solutions for the quadratic-cubic fractional nonlinear Schrödinger equation. *AIP Adv.* 2021;11(5):055105. https://doi.org/10.1063/5.0050624
34. Jiang X, Chen X, Chi M, Chen J. On Hopf bifurcation and control for a delay systems. *Appl Math Comput.* 2020;370:124906. https://doi.org/10.1016/j.amc.2019.124906
35. Lin J, Xu C, Zhao Y, Pang Y, Liu Z, Shen J. Bifurcation and control of a predator-prey system with two time delays. *J Appl Anal Comput.* 2026;16(2):807-859. https://doi.org/10.11948/20250164
36. Cinar M, Onder I, Secer A, Yusuf A, Sulaiman TA, Bayram M, *et al.* Soliton solutions of (2+1) dimensional Heisenberg ferromagnetic spin equation by the extended rational sine-cosine and sinh-cosh method. *Int J Appl Comput Math.* 2021;7(4):135. https://doi.org/10.1007/s40819-021-01076-5
37. Hamza AE, Suhail M, Alsulami A, Mustafa A, Aldwoah K, Saber H. Exploring soliton solutions and chaotic dynamics in the (3+1)-dimensional Wazwaz-Benjamin-Bona-Mahony equation: A generalized rational exponential function approach. *Fractal Fract.* 2024;8(10):592. https://doi.org/10.3390/fractalfract8100592
38. Farooq K, Tedjani AH, Li Z, Hussain E. Soliton dynamics of the nonlinear Kodama equation with M-truncated derivative via two innovative schemes: The generalized Arnous method and the Kudryashov method. *Fractal Fract.* 2025;9(7):436. https://doi.org/10.3390/fractalfract9070436
39. Ehsan H, Abbas M, Nazir T, Mohammed PO, Chorfi N, Baleanu D. Efficient analytical algorithms to study Fokas dynamical models involving M-truncated derivative. *Qual Theory Dyn Syst.* 2024;23(1):49. https://doi.org/10.1007/s12346-023-00890-0
40. Gu M, Liu F, Li J, Peng C, Li Z. Explicit solutions of the generalized Kudryashov's equation with truncated M-fractional derivative. *Sci Rep.* 2024;14(1):21714. https://doi.org/10.1038/s41598-024-72610-w
41. Li Z. Optical solutions of the nonlinear Kodama equation with the M-truncated derivative via the extended $(\frac{G'}{G})$-expansion method. *Fractal Fract.* 2025;9(5):300. https://doi.org/10.3390/fractalfract9050300
42. Ismael HF, Baskonus HM, Bulut H, Gao W. Instability modulation and novel optical soliton solutions to the Gerdjikov-Ivanov equation with M-fractional. *Opt Quantum Electron.* 2023;55(4):303. https://doi.org/10.1007/s11082-023-04581-7
43. Shakeel M, Alshammari FS, Ahmadzai HG. Optical soliton solutions, dynamical and sensitivity analysis for fractional perturbed Gerdjikov-Ivanov equation. *Sci Rep.* 2025;15(1):30843. https://doi.org/10.1038/s41598-025-09571-1
44. Rehman SU, Bilal M, Ren J, Bayram M, Inc M. Sensitivity analysis and dynamics of optical dromions in conformable generalized nonlinear Schrödinger systems. *Phys Lett A.* 2025;531:130168. https://doi.org/10.1016/j.physleta.2024.130168
45. Shahen NHM, Amin MA, Foyjonnesa, Rahman MM. Dynamics of computational waveform: A study of bifurcation, chaos, and sensitivity analysis. *PLoS One.* 2025;20(7):e0326230. https://doi.org/10.1371/journal.pone.0326230
46. Li P, Shi S, Xu C, Rahman MU. Bifurcations, chaotic behavior, sensitivity analysis and new optical solitons solutions of Sasa-Satsuma equation. *Nonlinear Dyn.* 2024;112(9):7405-7415. https://doi.org/10.1007/s11071-024-09438-6
47. Demirbilek U, Muhammad J, Akbulut A, Younas U, Radwan T, Ahmed KK. The dynamical landscape of the negative-order (3+1)-dimensional Calogero-Bogoyavlenskii-Schiff equation. *J Math.* 2026;2026(1):8273647. https://doi.org/10.1155/jom/8273647

Shafqat Ur Rehman *is an assistant professor of Applied Mathematics at the Department of Mathematics, Grand Asian University Sialkot. He received his Ph.D. in 2023 from the University of Gujrat for his research in the field of Applied Mathematics. As a researcher, his research interests include various analytical methods to extract exact solutions for nonlinear differential equations, mathematical physics, and nonlinear optics (including ordinary, partial, fractional-order, and stochastic) by using analytical and semi-analytical methods.*
https://orcid.org/0000-0001-7767-9785

Sekson Sirisubtawee *is an Associate Professor in the Department of Mathematics, Faculty of Applied Science, at King Mongkut's University of Technology North Bangkok, Thailand. He received his Ph.D. in Applied Mathematics from University of Colorado at Boulder, USA, in 2014. His research interests include numerical analysis, dynamical systems, mathematical modeling, and exact solutions of partial differential equations. His research work particularly focuses on nonlinear and fractional differential equations, traveling wave and solitary wave solutions, stability and bifurcation analysis, modulation instability, and mathematical modeling. He has published extensively on analytical and numerical methods for nonlinear evolution equations, fractional-order models, nonlinear Schrödinger equations, and related problems in applied mathematics.*
https://orcid.org/0000-0003-0715-470X

Khomsan Neamprem *serves as an Assistant Professor in the Department of Mathematics, Faculty of Applied Science, at King Mongkut's University of Tech-*

nology North Bangkok (KMUTNB), where he has been a faculty member since 2010. He earned his doctorate in Computational and Applied Mathematics from Old Dominion University in Virginia, USA. Prior to his Ph.D. studies, he received a Master of Science in Applied Mathematics from Mahidol University and a Bachelor of Science in Applied Mathematics with First Class Honors from KMUTNB. His primary research interests focus on numerical analysis and numerical solutions of integral and differential equations.
https://orcid.org/0000-0003-0930-4943

Chaiyod Kamthorncharoen *received the M.Sc. degree in Applied Mathematics and Computational Science from Chulalongkorn University, Thailand, in 2014, and the Ph.D. degree in Computer Science from Heidelberg University, Germany, in 2022. He is currently affiliated with the Department of Mathematics, Faculty of Applied Science at King Mongkut's University of Technology North Bangkok (KMUTNB), Thailand. His primary research interests center on the numerical solution of partial differential equations, with specific expertise in finite element and discontinuous Galerkin methods, domain decomposition, and nonlinear preconditioning. He has authored research articles in international peer-reviewed journals and conference proceedings.*
https://orcid.org/0009-0006-6743-7356

Appendix

For validating **Equation (1)** by replacing **Equation (6)**. Replacing **Equation (6)** into **Equation (1)** gives

$$
\begin{aligned}
&b_1 = 0,\\
&\zeta = \frac{\Gamma(\beta+1)}{\alpha}(x^\alpha - \nu t^\alpha),\\
&\Theta = \frac{\Gamma(\beta+1)}{\alpha}(-\kappa x^\alpha + \omega t^\alpha) + \theta_0,\\
&u_1 = -\frac{ie^{i\Theta}\sqrt{a\kappa^2+\omega}}{\sqrt{b_2}}\cot\left(\frac{\zeta\sqrt{a\kappa^2+\omega}}{\sqrt{2a}}\right),\\
&u_{m1} = -\frac{i\sqrt{a\kappa^2+\omega}}{\sqrt{b_2}}\cot\left(\frac{\zeta\sqrt{a\kappa^2+\omega}}{\sqrt{2a}}\right),\\
&\nu = -2a\kappa,\\
&\text{sol1} = \text{Simplify}\Bigg[\frac{t^{1-\alpha}}{\Gamma(1+\beta)}i\frac{\partial u_1}{\partial t}\\
&\qquad + \frac{ax^{1-\alpha}}{\Gamma(1+\beta)}\frac{\partial}{\partial x}\left(\frac{x^{1-\alpha}}{\Gamma(1+\beta)}\frac{\partial u_1}{\partial x}\right)\\
&\qquad - b_1 u_{m1}u_1 + b_2(u_{m1})^2 u_1 = 0\Bigg]\text{//Simplify}
\end{aligned}
$$

True.

The variable u_1 means complete solution of given PDE and u_{m1} denotes modulus values of u_1. Similarly the remaining solutions can also be verified.

An International Journal of Optimization and Control: Theories & Applications (https://accscience.com/journal/ijocta)



This work is licensed under a Creative Commons Attribution 4.0 International License. The authors retain ownership of the copyright for their article, but they allow anyone to download, reuse, reprint, modify, distribute, and/or copy articles in IJOCTA, so long as the original authors and source are credited. To see the complete license contents, please visit http://creativecommons.org/licenses/by/4.0/.